JCI insight

Multi-omics of Bohring-Opitz syndrome truncating *ASXL1* mutations identify canonical and non-canonical Wnt signaling dysregulation

Isabella Lin, … , Rosanna Weksberg, Valerie A. Arboleda

JCI Insight. 2023. https://doi.org/10.1172/jci.insight.167744.

Research In-Press Preview **Development** **Genetics**

ASXL1 (*Additional sex combs-like 1*) plays key roles in epigenetic regulation of early developmental gene expression. De novo truncating mutations in *ASXL1* cause Bohring-Opitz syndrome (BOS, OMIM #605039), a rare neurodevelopmental condition characterized by severe intellectual disabilities, characteristic facial features, hypertrichosis, increased risk of Wilms tumor, and variable congenital anomalies including heart defects and severe skeletal defects giving rise to a typical 'BOS posture'. These BOS-causing *ASXL1* variants are also high-prevalence somatic driver mutations in acute myeloid leukemia (AML). We use primary cells from BOS individuals (n = 18) and controls (n = 49) to dissect gene regulatory changes caused by *ASXL1* mutations using comprehensive multi-omics assays for chromatin accessibility (ATAC-seq), DNA methylation, histone methylation binding, and transcriptome in peripheral blood and skin fibroblasts. Our data shows that regardless of cell type, *ASXL1* mutations drive strong cross-tissue effects that disrupt multiple layers of the epigenome. The data showed a broad activation of canonical Wnt signaling at the transcriptional and protein levels and upregulation of *VANGL2*, a planar cell polarity pathway protein that acts through non-canonical Wnt signaling to direct tissue patterning and cell migration. This multi-omics approach identifies the core impact of *ASXL1* mutations and therapeutic targets for BOS and myeloid leukemias.

Multi-omics of Bohring-Opitz syndrome truncating *ASXL1* mutations identify canonical and non-canonical Wnt signaling dysregulation

Isabella Lin[1,2,3], Angela Wei[1,2,3,4], Zain Awamleh[5], Meghna Singh[1,2,3], Aileen Ning[1,2,3], Analeyla Herrera[1,2,3], REACH Biobank and Registry[1], Bianca E. Russell[6], Rosanna Weksberg[5,7,8], Valerie A. Arboleda[1,2,3,4,9,10]

1 Department of Human Genetics, David Geffen School of Medicine, University of California, Los Angeles, CA, USA
2 Department of Pathology and Laboratory Medicine, David Geffen School of Medicine, University of California, Los Angeles, CA, USA
3 Department of Computational Medicine, David Geffen School of Medicine, University of California, Los Angeles, CA, USA
4 Interdepartmental BioInformatics Program, University of California, Los Angeles, CA
5 Department of Genetics and Genome Biology Program, Research Institute, The Hospital for Sick Children, Toronto, ON M5G 0A4, Canada
6 Department of Pediatrics, Division of Genetics, University of California, Los Angeles, UCLA
7 Division of Clinical & Metabolic Genetics, The Hospital for Sick Children, Toronto, ON M5G 1X8, Canada
8 Institute of Medical Sciences and Department of Molecular Genetics, University of Toronto, Toronto, ON MS5 1A8, Canada
9 Molecular Biology Institute, University of California, Los Angeles, CA
10 Jonsson Comprehensive Cancer Center, University of California, Los Angeles, CA

Corresponding Author:
Valerie A. Arboleda MD PhD
varboleda@mednet.ucla.edu
Phone: 310-983-3568
615 Charles E. Young Drive South
Los Angeles, CA 90095

ABSTRACT

ASXL1 (*Additional sex combs-like 1*) plays key roles in epigenetic regulation of early developmental gene expression. *De novo* truncating mutations in *ASXL1* cause Bohring-Opitz syndrome (BOS, OMIM #605039), a rare neurodevelopmental condition characterized by severe intellectual disabilities, characteristic facial features, hypertrichosis, increased risk of Wilms tumor, and variable congenital anomalies including heart defects and severe skeletal defects giving rise to a typical 'BOS posture'. These BOS-causing *ASXL1* variants are also high-prevalence somatic driver mutations in acute myeloid leukemia (AML). We use primary cells from BOS individuals (n=18) and controls (n=49) to dissect gene regulatory changes caused by *ASXL1* mutations using comprehensive multi-omics assays for chromatin accessibility (ATAC-seq), DNA methylation, histone methylation binding, and transcriptome in peripheral blood and skin fibroblasts. Our data shows that regardless of cell type, *ASXL1* mutations drive strong cross-tissue effects that disrupt multiple layers of the epigenome. The data showed a broad activation of canonical Wnt signaling at the transcriptional and protein levels and upregulation of *VANGL2*, a planar cell polarity pathway protein that acts through non-canonical Wnt signaling to direct tissue patterning and cell migration. This multi-omics approach identifies the core impact of *ASXL1* mutations and therapeutic targets for BOS and myeloid leukemias.

Brief summary

Germline *ASXL1* mutations that cause Bohring-Optiz syndrome disrupt the epigenome and dysregulate gene expression resulting in activation of canonical and non-canonical Wnt signaling pathways.

Keywords:

Genomics, Epigenome, ASXL1, Multiomics, Bohring-Opitz Syndrome

INTRODUCTION

ASXL1 (Additional sex combs-like 1) is an essential protein in embryonic development (1). Eutherian mammals have three *Asx* homologs, *ASXL1, ASXL2,* and *ASXL3,* which share conserved domains; the ASX N-terminal (ASXN) domain with a HARE-HTH domain involved in putative DNA binding (2), the ASX homology (ASXH) domain with a characteristic LXXLL motif that mediates protein interactions and DEUBAD domain that activates BAP1, and the C-terminal plant homeodomain (PHD) important in “reading” post-translational histone modifications such as histone H3 Lys4 trimethylation (H3K4me3) (3–5) (Figure 1A). *ASXL1* plays a role in the modulation of the epigenetic landscape which regulates downstream transcription. The ASXH and PHD domains are highly conserved and are part of large epigenetic complexes, the Polycomb (PcG) complexes and the Deubiquitinase complexes. These epigenetic complexes direct genome-wide transcriptional regulation (3, 6, 7) through activation or repression of essential developmental genes. *Asx,* the *Drosophila melanogaster* ortholog, plays a critical role in anterior-posterior patterning (8) and mutant embryos exhibit incomplete head involution and posterior directed transformations of all abdominal segments (8). In mammals, *ASXL1* is essential in early neural crest (9), cardiac (10) and hematopoietic development (11, 12).

ASXL1 directs histone modifications through the Polycomb Repressive Complex 1 and 2 (PRC1/2) and the Polycomb Repressive Deubiquitinase complex (PR-DUB). PRC1 and 2 control activation of developmental stemness and differentiation, including progressive restriction of neural progenitor cell multipotency and production of mature cortical neurons during corticogenesis (13). This control of the stem-cell state occurs through monoubiquitination at histone H2A lysine 119 (H2AK119ub) via PRC1 and mono-, di-, and tri-methylation at histone H3K27 (H3K27me, H3K27me2, H3K27me3) via PRC2 (3, 14, 15). Together, these complexes regulate key signaling pathways such as Wnt signaling in tissue-specific and developmental contexts, with PRC2 accessory proteins regulating Wnt signaling during erythropoiesis (16) and

PRC1 regulating the Wnt/β-catenin pathway through a positive feedback loop in hepatocellular carcinoma (HCC) (17).

The PR-DUB, which includes ASXL1 that binds BRCA1-associated protein 1 (BAP1) (18–20), plays key roles in brain development (21–23) and regulation of myeloid differentiation through H2AK119 deubiquitination (19, 24). While it is clear that *ASXL1* protein truncating mutations disrupt core developmental processes across multiple organ systems, its role as an essential chromatin modifier in human development has not been fully elucidated.

ASXL1 mutations in Bohring-Opitz Syndrome (BOS) and in hematologic malignancies.

De novo protein truncating mutations of *ASXL1* cause a rare genetic disorder, Bohring-Opitz Syndrome (BOS, OMIM #605039). BOS is characterized by profound intellectual disability, developmental delay, seizures, variable anomalies including heart defects, higher risk of Wilms tumor, and 'BOS posture' (25, 26). As of 2018, only 46 clinically diagnosed individuals have been reported in the literature, with less than half (20/46) molecularly confirmed (25). Pathogenic truncating mutations in *ASXL1* are enriched in exons 12 and 13, the penultimate and ultimate exons (3), resulting in premature truncation of the highly conserved C-terminal PHD domain. Intriguingly, truncation mutations in *ASXL1* homologs *ASXL2* (Shashi-Pena Syndrome, OMIM#6171901) (27) and *ASXL3* (Bainbridge-Ropers Syndrome, OMIM #615485) (23, 28) are not enriched or clustered in the homologous C-terminal region despite sharing multiple conserved domains (3).

The same protein-truncating mutations causing BOS are also observed as somatic driver mutations in myeloid malignancies such as chronic myelomonocytic leukemia (CMML, ~45%), myelodysplastic syndromes (MDS, 16%), myeloproliferative neoplasms (~10%) and acute myeloid leukemia (AML, secondary 30%, *de novo* 6.5%) (29–32). Studies have identified low-frequency somatic mutations in *ASXL1* correlated with mutagenic processes and increasing age (33), defining a new pre-malignancy state called clonal hematopoiesis of indeterminate potential

(33, 34). *ASXL1* regulates the delicate interplay between proliferation and differentiation of stem progenitor cell populations (9, 35) and therefore, both germline and somatic *ASXL1* mutations disrupt the proliferation-differentiation balance and promote stem-cell identity over differentiation in BOS and myeloid leukemias.

Recent *ASXL1* functional studies have been carried out as transgenic overexpression of mutant and wild-type ASXL1 proteins in cell-line systems. These studies are difficult to interpret because they are not reflective of endogenous levels or cell-type specific functions of ASXL1 or they are in non-human model systems (36). Given the multiple essential functions of *ASXL1* as part of PRC1 and PRC2 in neural progenitor multipotency (13), and key role of PR-DUB in brain development (21–23), we hypothesize that protein truncating mutations of *ASXL1* dysregulate global transcription, cellular homeostasis and downstream signaling pathways.

We also examined whether BOS cells harbored decreased mRNA or protein levels since protein truncating ASXL1 mutations occur in the last two exons of the gene, exons 12 and 13, and are predicted to escape nonsense mediated decay (37). These truncated proteins are predicted to have a gain-of-function effect (38). The broad phenotypic effects of *ASXL1* mutations in BOS patients and myeloid malignancies suggest that *ASXL1* drives essential and core gene regulatory features across early development and disease. We hypothesized that *ASXL1* mutations share common cellular effects that might therefore be detectable as broad and high-effect epigenomic and transcriptomic signatures across cells and tissues.

To study BOS molecular pathogenesis, we collected samples from 18 BOS patients, one of the largest ASXL rare disease cohorts published, and performed multi-omics analysis. Our approach circumvents the confounding variable of cancer-derived cell models that harbor multiple additional karyotypic and genomic mutations (31, 39) and focuses our study on the singular effect of pathogenic *ASXL1* mutations. This integrated multi-omics study characterizes the impact of *ASXL1* truncating mutations on the epigenome and transcriptome and our work shows for the first

time that *ASXL1* mutations aberrantly activate Wnt signaling pathway and non-canonical Wnt planar cell polarity (PCP) genes.

The canonical Wnt signaling is an evolutionarily-conserved signaling pathway that is essential for development (40), and plays important roles in stem cell biology and regulation of hematopoiesis (41). In the Wnt-active state, WNTs (translated products of WNT gene) bind to the transmembrane receptor Frizzled (FZD) and stimulate the co-receptor Low Density Receptor-Related Protein (LRP)5/6, which play critical roles in initiation of Wnt signaling transduction (42). Activation of FZD and LRP5/6 recruits and inactivates the "destruction complex" that targets phosphorylation, ubiquitination and degradation of β-catenin through the proteasome. Inactivation of the "destruction complex" occurs through dissociation of glycogen synthase kinase 3 beta (GSK3B) from Axin inhibition protein (AXIN), and concurrent inactivation of the default quiescent-state "β-catenin destruction complex" (43–45). This means that β-catenin cannot be phosphorylated, and thus cannot be degraded (46, 47). The activation of the canonical Wnt pathway results in cytoplasmic accumulation and subsequent nuclear translocation of β-catenin which, along with T-cell factor/lymphoid enhancer factor (TCF/LEF) transcription factors transcriptionally co-activates Wnt-target genes (48).

To examine cross-omics dysregulation in more depth, we explored Van gogh-like 2 (*VANGL2)*, a non-canonical Wnt and planar cell polarity (PCP) protein, which was highly dysregulated across all the -omics assays conducted across blood and fibroblast BOS samples. *VANGL2* regulates polarized cellular migration and differentiation and tissue morphology during development. In the nervous system, the PCP pathway regulates neuronal maturation and has a functional role in neural complex formation (49). VANGL2 intersects with the canonical pathway through activation of DVL which activates non-canonical pathways and drives c-JUN mediated expression. We hypothesize that upregulation of *VANGL2* disrupts canonical and non-canonical signaling pathways and underlies the clinical phenotypes observed in patients with BOS and other

mutations in *ASXL*. To date, no studies have established a link between *ASXL1* disorders and dysregulation of Wnt-signaling.

In this study, we identify and test the mechanisms by which truncating *ASXL1* mutations in BOS may dysregulate the canonical and non-canonical Wnt signaling pathways. These findings elucidate novel regulatory mechanisms underlying BOS pathogenesis.

RESULTS

Study Design. We recruited 18 individuals with BOS (Supplemental Table 1), 25 sex-matched and genetically related controls to account for genetic variation, and 30 sex- and age- matched controls (Supplemental Table 2). This is the largest cohort of BOS patients studied at the molecular level, and includes novel patients first reported in 2023 by Russell et al. (50). All BOS individuals have clinically identified *ASXL1* mutations in the last two exons of the gene that are predicted to cause protein truncating variants (NM_015338.6) between amino acids 364 to 1415 (Figure 1A, Supplemental Table 1). All mutations were verified through bulk RNA-seq data visualization in IGV (Supplemental Figure 1) to confirm specimen identity. A summary of patient demographics are detailed in Supplemental Table 3. Clinical data of this cohort are available through the ASXL registry, and a subset of patients were previously reported by Awamleh et al. (51).

Consented individuals donated peripheral blood (n=14), a skin punch biopsy (n=8) or both. We obtained both sample types from 4 of the 18 BOS individuals in this study which allowed us to integrate data across sample types to identify tissue-dependent and -independent dysregulation caused by truncating *ASXL1* mutations. We used primary sample types to examine the direct role of the mutation on patient tissue. We used controls with similar genetic backgrounds to control for baseline genetic effects. We conducted a comprehensive multi-omics analysis across tissues (Figure 1B). We assessed global changes to the epigenome using three approaches: chromatin accessibility using assay for transposase-accessible chromatin using

sequencing (ATAC-seq) (52), H3K4me3 and H3K27me3 enrichment using cleavage under targets and release using nuclease (CUT&RUN) (53), and the DNA methylation (DNAm) landscape through Illumina Epic Arrays (51). Not all samples were assessed by all methods and therefore the overlap between assays for BOS individuals is outlined in Figure 1C. We derived disease-specific DNAm signatures (51) and transcriptional signatures from RNA-seq using blood and fibroblast cells (Figure 1B), and integrated our findings to examine the trans-omics dysregulation (Figure 1D).

ASXL1 is expressed across multiple tissues and multiple cell types (Supplemental Table 4), consistent with the clinical phenotype spanning multiple organ systems. To test our hypothesis that *ASXL1* mutations may have high-level epigenomic and transcriptomic signatures across affected cells and tissues, we conducted RT-qPCR using *ASXL1* primers (Supplemental Table 5). We found no significant differences in *ASXL1* expression levels between representative BOS (n=4) and control (n=4) blood samples (Supplemental Figure 2A) or between representative BOS (n=6) and control (n=6) fibroblast samples (Supplemental Figure 2B). For blood samples, the RNA-seq *ASXL1* transcript fold change (|log2FoldChange|) was 0.11, which did not meet our threshold of 0.58 for strong fold change, and the adjusted p value (p_{adj}) was 0.29, which did not meet our significance threshold of $p_{adj}<0.05$ (Supplemental Figure 2C). Similar, for fibroblasts, the |log2FoldChange| (abs(log2FC)) was -0.01 and p_{adj} was 0.95 (Supplemental Figure 2D).

We next asked if the truncating mutation caused differences in wild-type ASXL1 protein levels due to decreased translational efficiency or stability of the truncated allele. We identified a high quality antibody by testing multiple, commercially-available antibodies (Supplemental Table 6, Supplemental Figure 3A) in CACO2 cells, a cell line with very high *ASXL1* RNA expression (Supplemental Table 4), and HEK293T cells transfected with FLAG-tagged truncated *ASXL1* (54). We identified two antibodies (ab228009, MABE1933) that showed bands at the same molecular weight of 75 kDA, one of which (ab228009) showed higher expression of ASXL1 in CACO2 cells and overlapped with ASXL1-construct with high-affinity FLAG antibody (Supplemental Figure 3B).

Western blot for ASXL1 identified no significant difference in total ASXL1 protein levels between BOS (n=5) and control (n=5) fibroblasts (Figure 1E, Supplemental Figure 4, Supplemental Table 7). Western blot bands for ASXL1 were detected at the same molecular weight between BOS and control samples, and truncated proteins were not detected at a reduced molecular weight for any BOS sample tested. This is consistent with other literature examining endogenous, truncated human ASXL1 expression (55).

Finally, we extracted histones from fibroblast cells and quantified global changes for histone modification. The mutations in BOS terminate ASXL1 before the PHD domain, a histone- or DNA-binding domain reported to recognize a subset of histone modifications including H3K4me and H3K27me3 (5), and thought to affect levels of H3K27me3 and H2AK119ub (19). We performed histone immunoblotting for these specific modifications using representative BOS (n=5) and control (n=5) fibroblast and do not observe any significant changes to H3K4me3, H3K27me3, or H2AK119Ub levels (Figure 1F, Supplemental Figure 5, Supplemental Table 7)

Transcriptomic analysis identifies transcriptional pathways disrupted in BOS

One of the core functions of *ASXL1* is to activate the epigenome to express certain genes and pathways at developmental timepoints. Changes to the epigenome activate or repress transcription and RNA-seq can identify the effects of the transcriptional rewiring due to epigenetic mutations. To address this, we performed RNA-seq in blood and dermal fibroblasts from individuals with BOS and controls. Transcriptomic data was generated to a minimum of 30 million reads per sample for a total of 33 RNA-seq libraries: 8 BOS-blood, 7 BOS fibroblasts, 11 control blood, and 7 control fibroblasts (Supplemental Table 8 and 9, Methods). Similar to the qRT-PCR data, *ASXL1* normalized gene expression was not significantly different between BOS (n=8) and control (n=11) blood, or between BOS (n=7) and control (n=7) fibroblast samples (Supplemental Figures 2C and 2D). We identified that increased number of ASXL1 reads was correlated with total sequencing reads in both blood samples and fibroblast samples as expected (Supplemental

Figure 6A). Fibroblast samples had higher normalized ASXL1 read counts per sequencing coverage compared to blood samples, which is expected given ASXL1 expression by tissue type (Supplemental Table 4).

We then examined whether the total number of reads at each BOS sample's mutation site was correlated with total ASXL1 reads (Supplemental Figure 6B). We identified a minimum of 1195 and a maximum of 5612 ASXL1 reads per sample. Here, we found no significant correlation between ASXL1 reads at mutation site and total ASXL1 reads; $R^2<0.01$ for blood samples and $R^2=0.10$ for fibroblast samples. While Pt4 fibroblasts were identified to have only 2 reads at the mutation site compared to a total of 3968 total ASXL1 reads, Pt8 blood were identified to have 100 reads at the mutation site compared to a total of 1314 ASXL1 reads (Supplemental Tables 8-10).

We also calculated whether the *ASXL1* reference and mutant alleles were equally represented in patient blood (Figure 2A, n=8) and fibroblast (Figure 2B, n=7) RNA-seq data. We calculated the variant allele frequency (VAF) at the mutation site across each BOS sample (Supplemental Figure 7). For germline disorders, we would expect the VAF of the mutant allele to represent between 30 to 70 percent of the reads covering the mutation site ($0.3<VAF<0.7$). Most BOS samples fell within the expected germline range (Figures 2A and 2B, Supplemental Table 10), suggesting that these late-truncating alleles escape nonsense-mediated decay.

One key exception to the expected germline allele distribution was Pt6, with truncating mutation at amino acid 672 who had undergone treatment with actinomycin D and vincristine for Wilms tumor years prior to sample collection. In fibroblast RNA-seq, this sample had an *ASXL1* allele ratio of 36.9% pathogenic allele, which is within expected germline levels. However, in Pt6's blood RNA-seq, 100% of reads (27/27) over the *ASXL1* mutation contained the pathogenic mutation and no reference allele was identified. This loss of heterozygosity may have occurred as a selective growth advantage during tumorigenesis, during treatment or could represent new clonal hematopoiesis.

To assess the pathogenesis of truncating *ASXL1* mutations, we examined the effects on global transcription across different tissues. *ASXL1* is ubiquitously expressed across the body at low levels, and is more highly expressed in skin (32.55 TPM) than in whole blood (8.03 TPM) (Supplemental Table 4). We expected a much higher number of significant differentially expressed genes (DEGs) in blood RNA-seq than in fibroblast RNA-seq because blood RNA represents a bulk assessment of heterogeneous cell types which can introduce an extra source of differential expression. We see significantly more gene expression dysregulation in blood with 2118 significant DEGs (Figure 2C) compared to fibroblast RNA-seq with 177 significant DEGs (Figure 2D). Complete lists of DEGs in each dataset are in Supplemental Table 11 for BOS fibroblast and Supplemental Table 12 for BOS blood.

We identified an outlier in our RNA-seq analysis of blood samples; Pt7 (Figure 2C). Age 29 at sample collection (Supplemental Table 1), Pt7 was one of the very few 'older' patients given that BOS is associated with high infant mortality (27%) and most patients do not survive into early adulthood (56). Given the extremely low prevalence of BOS and selection of donated samples, the sample size restricted our ability to independently assess Pt7 for effects of age. Furthermore, collecting samples from age-matched controls is difficult given that matched controls would be young, healthy children. We strove to correct for the effects of age through including an age-matched control, Ctrl19 at age 28 (Supplemental Table 2), integration of analyses across different -omics assays with a range of control group ages, and assessment of significant genes against any age-specific bias. Furthermore, significant genes that are identified for RNA-seq blood analysis in this text were examined to see if Pt7 had transcript expression more similar to other BOS cases before downstream analysis.

After filtering for fold change ($|\log2FC| \geq 0.58$), we see 1097 significant DEGs in blood and 155 significant DEGs in fibroblasts. Both RNA-seq analysis of blood and fibroblasts identified larger proportions of DEGs that are upregulated in BOS patients than in controls. In blood, 590/1097 DEGs (53.8%) were upregulated (Figure 2C), and in fibroblast cells 125/155 DEGs

(80.6%) (Figure 2D). In blood, top DEGs included *GRIK5* (Glutamate receptor, Kainate 5, $log_2FC=3.8$), *VANGL2* (Vang-like protein 2, $log_2FC=3.8$), and *GREM2* (Gremlin 2, BMP antagonist, $log_2FC=-2.5$). Top DEGs in the fibroblast RNA-seq dataset include *UGT3A2* (UDP Glycosyltransferase Family 3 Member A2, $log_2FC=4.8$), *VANGL2* ($log_2FC=2.5$), *GRIK5* ($log_2FC=2.5$) and *GREM2* ($log_2FC=-2.1$). Gene ontology analyses were performed using the list of significant DEGs. Despite neither tissue being neural in origin, regulation of neuron projection development ($p_{adj}=9.82x10^{-5}$ in blood, $p_{adj}=0.02$ in fibroblasts) was identified as a gene ontology biological process enriched in both BOS tissues (Figure 2E and2F, Supplemental Tables 13 and 14). These enrichments were driven by genes that play key roles in early morphogenesis, particularly neurodevelopmental processes.

Our findings from gene ontology analyses in blood and fibroblast also identified some gene expression changes that are tissue-specific. Blood DEGs were enriched for hematological processes such as T-cell activation ($p_{adj}= 3.23x10^{-8}$), neutrophil activation ($p_{adj}=1.90x10^{-5}$), axogenesis ($p_{adj}=1.90x10^{-5}$), leukocyte cell-cell adhesion ($p_{adj}=3.62x10^{-5}$) (Figure 2E, Supplemental Table 13). Fibroblast DEGs were enriched for structural cell processes such as dysregulation of potassium ion transport ($p_{adj}=0.004$) and regulation of membrane potential ($p_{adj}=0.02$) (Figure 2F, Supplemental Table 14).

To examine potential common, cross-tissue effects of truncating *ASXL1* mutations, we correlated all our BOS blood RNA-seq DEGs and all our BOS fibroblast RNA-seq DEGs to identify shared dysregulated transcripts (Figure 2G). We identified a core subset of 25 genes dysregulated across both tissue types, with 21/25 (84%) DEGs dysregulated in the same direction, suggesting a strong tissue-independent *ASXL1* effect that supersedes tissue type. Notable genes include *VANGL2, GRIK5* and *GREM2*.

Differential chromatin accessibility in BOS allows for aberrant activation of developmental and morphogenic pathways.

To correlate gene expression profiles with chromatin accessibility (Figure 1D), ATAC-seq was performed on BOS (n=6) and control (n=6) fibroblast cells. Chromatin accessibility, identified by increased reads over a genomic region in ATAC-seq, positively correlated with gene expression (52, 58).

All ATAC-seq libraries had the expected distribution of fragment lengths, with an average of 52% of fragments being small (<200 bp length) representing open chromatin regions, and progressively fewer fragments of larger size spanning nucleosomes (>300 bp length) (Supplemental Figure 8, Supplemental Table 15). Of note, BOS patient fibroblasts had a mean insert size of 184bp, representing more open chromatin regions, while control fibroblasts had a median insert size of 242bp, representing less open chromatin regions. PCA identified clear separation of BOS and control samples on PC1 (47% variance) (Supplemental Figure 9A), as did heatmap analysis of the significant peaks (Figure 3A). 4336 significant peaks (p_{adj}>0.05, abs(log_2FC)>0.58) corresponding to differentially accessible regions were identified, with 3036 peaks (70.02%) more differentially open and 1300 peaks (29.98%) more closed in BOS patients compared to controls (Supplemental Figure 9B, Supplemental Table 16). This mapped to a total of 3054 unique genes, with 763/3054 genes (25.0%) represented by more than one significant differentially accessible peak (Supplemental Table 17). These included *APBA2 (Amyloid beta precursor protein binding family A member 2)* represented by 8 peaks, *KCNQ5* (Potassium voltage-gated channel subfamily Q member 5) represented by 3 peaks, and *OTUD7A* (OTU deubiquitinase 7A), *PRXL2A* (Peroxiredoxin like 2A) and *PELI2* (Pellino E3 ubiquitin protein ligase family member 2) each represented by 2 peaks. Peaks were annotated using HOMER to the nearest gene or regulatory element (see Supplemental Methods) (57, 59). Top differentially accessible peaks mapped to *FBXL20* (log_2FC=-8.3), *LINGO1* (log_2FC=-7.2), *RUNX3* (log_2FC=4.4) and *CTNNB1* (gene encoding β-catenin, log_2FC=3.8).

We identified gene set enrichments in multiple key developmental systems including muscle development and differentiation (p_{adj}=9.11x10^{-13}), skeletal system development

(p_{adj}=1.0x10^{-9}), regulation of neurogenesis (p_{adj}=1.35x10^{-9}), limb morphogenesis (p_{adj}=1.38x10^{-8}), renal system development (p_{adj}=2.14x10^{-8}), and cardiac septum morphogenesis (p_{adj}=2.67x10^{-8}) (Figure 3B, Supplemental Table 18). Key motifs that were identified in the differentially accessible chromatin regions of our ATAC-seq data suggest core factors that drive dysregulation of the DEGs. Motif enrichment analysis of our ATAC-seq data using both known motif and *de novo* methods identified significant enrichment of the following transcription factor binding sites: JunB (p_{adj}=1x10^{-208}, BOS 18.43%, background 5.23%), RUNX1 (p_{adj}=1x10^{-203}, BOS 26.45%, background 10.09%) and Fra1 (p_{adj}=1x10^{-196}, BOS 17.44%, background 4.95%) (Supplemental Table 19).

Chromatin accessibility is correlated with dysregulation of gene expression in BOS.

To determine whether some of the transcriptional dysregulation identified in BOS occurs through chromatin accessibility, we integrated DEGs from fibroblast RNA-seq (BOS n=6, control n=6) with differentially accessible chromatin regions identified through ATAC-seq (BOS n=6, control n=6). This revealed a positive correlation (R^2=0.405) between increased chromatin accessibility and increased gene expression of the same gene (Figure 3C). 71 differentially accessible chromatin regions aligned to 37/117 unique DEGs (20.9%) in the fibroblast RNA-seq dataset (Supplemental Table 20). Where a DEG was represented by more than one significantly differentially accessible peak, we confirmed that the peaks were concordant in direction of change. A subset of these peaks mapped to the promoter-TSS (transcriptional start site) region, which usually indicate stronger effects on transcription. 14/71 (19.7%) peaks mapped to promoter-TSS regions, including the differentially accessible peak for *VANGL2. This* corresponded to 13/37 (35.1%) unique DEGs in the fibroblast RNA-seq data (Supplemental Figure 10). These peaks showed a clear association of increased promoter accessibility and increased transcription.

A subset of the DEGs identified through ATAC-seq translated across tissue types and were also found to be dysregulated in RNA-seq of BOS fibroblast and blood samples (Table 1).

We identified seven genes that were significant and differentially expressed across omics levels (ATAC-seq and RNA-seq) and across tissues (blood and fibroblasts); *VANGL2, PRXL2A, APBA2, OTUD7A, KCNQ5, PELI2* and *GREM2* (Supplemental Figures 11-13). These genes play significant roles in body patterning, neuron function, neural plate development and ubiquitination among other functions.

Truncating *ASXL1* mutations dysregulate DNA methylation, and contribute to changes in gene expression

Endogenous CpG methylation levels at promoter regions are negatively correlated with gene expression (Figure 1D) (58). Thus, increased DNA CpG methylation or more closed chromatin are correlated with lower gene expression. To generate a BOS-specific DNA methylation (DNAm) signature, we profiled genome-wide DNAm in blood from BOS individuals (n=13) compared to sex- and age-matched control subjects (n=26) (Supplemental Table 2) (51). DNAm identified 8596 differentially methylated CpG sites (FDR<0.05) associated with an ENSEMBL gene, with 5773 CpG sites overlapping genes and mapping to 3803 unique genes. 763 differentially methylated CpG sites met a threshold of $|\Delta\beta|>0.10$ (10% DNAm difference) using linear regression modeling (Supplemental Table 21). These 763 differentially methylated CpG sites mapped to 163 unique genes, with 71/163 genes (43.6%) genes represented by more than one differentially methylated CpG site. After further filtering for effect size at a threshold of abs(log2FC)>0.58, we found 24 unique genes remaining, represented by 50 differentially methylated CpG sites, including Proteasome 20S subunit alpha 8 (*PSMA8*) represented by 8 sites, Ellis van Creveld (*EVC*) represented by 6 sites, and *LRP5* represented by 3 sites (Supplemental Table 22).

To examine the likelihood of statistically significant differential methylation resulting in downstream transcriptional effects, we correlated BOS blood DNAm and RNA-seq expression profiles. Endogenous CpG methylation levels at promoter regions are negatively correlated with

gene expression (58) (Figure 1D). We first identified differentially methylated CpG sites (FDR<0.05) and DEGs from RNA-seq (p_{adj}<0.05) separately. We found 672 differential CpG sites that mapped to 341 unique DEGs in the blood RNA-seq dataset, with 143 genes represented by more than one differential CpG site (Supplemental Table 23). Genes represented by more than one CpG site were analyzed for concordance across the same gene and analyzed in correlation with gene expression values for each individual sample. We filtered for highly differentially methylated sites (|Δβ|>5%) and highly differentially expressed transcripts (|log_2FoldChange (log_2FC)|>1.5). After filtering, we retained 50/672 CpG sites (7.44%) which corresponded to 24/341 unique genes (7.04%) (Figure 4A). 11 genes were represented by >1 CpG site, including *PSMA8* with 8 CpG sites and *GRIK5* with 2 CpG sites. *VANGL2* was represented by 1 CpG site. The correlation between these DNA methylation differences and transcriptomic changes indicates a steady-state effect of dysregulated DNA methylation on gene expression.

Three differentially methylated CpG sites, within the TSS, were identified for EVC and EVC2. EVC and EVC2 were both hypomethylated at the TSS (-5% and -3.5% respectively) and transcriptionally upregulated (log2FC= 1.50 and 1.54 respectively) in BOS patient blood.

We also generated BOS DNAm data using BOS (n=8) and control fibroblasts (n=8). DNAm identified 444 CpG sites at a nominal p-value of 0.005 and |Δβ|>0.10 (Supplemental Table 24). These CpG sites did not pass FDR<0.05 so were not considered significant. Compared to blood, the fibroblast DNAm analysis showed significantly lower significance and effect level, which is consistent with our RNA-seq findings between blood and fibroblasts. This is likely a result of the homogeneity that is inherent to fibroblast cell culture compared to the heterogeneity of primary tissue, in particular blood. This, in conjunction with the reduced number of DEGs identified in fibroblast RNA-seq already, compared to blood RNA-seq, likely resulted in no significant correlations between fibroblast DNAm and RNA-seq.

Gene set enrichment analysis of DNA methylation and RNA sequencing identifies activation of canonical Wnt pathway signaling in BOS samples.

The overlapping findings from the DNAm and RNA-seq datasets prompted us to run gene ontology analysis for common gene targets, using two complementary methods, GREAT (60) and clusterProfiler *v3.12.0 (61)*. We filtered for gene ontologies with $p_{adj}<0.05$ for significance. In both analyses, significant gene set enrichments were identified in the Wnt signaling pathway (GO#0060070, 17 genes, $p_{adj=}0.045$), anterior-posterior pattern specification process (GO#0007389, 19 genes, $p_{adj=}0.045$), and regulation of neuron projection development (GO#0010975, 19 genes, $p_{adj=}0.045$), among other biologically relevant pathways (Figure 4B, Supplemental Table 25). Key genes that are enriched for these pathways include *PSMA8, WNT7A, FZD3, LRP5* and *LRP6* in canonical Wnt signaling and body pattern specification. The latter pathway enrichment was also driven by strong dysregulation in *VANGL2.* These overlapping gene targets and pathways between methylome and transcriptome in BOS patients suggest strong, coordinated, epigenetically-driven effects of truncating *ASXL1* mutations.

PSMA8 is a key driver gene in the canonical Wnt-signaling enrichment identified in blood DNA methylation and RNA-seq data. We identified significant hypermethylation of *PSMA8* across all 8 CpG sites identified across the promoter and TSS region with Δβ from 6.1% to 18.9% (Figure 4C, Supplemental Figure 14A - 14F). *PSMA8* was also downregulated at the transcriptional level in BOS patient blood ($log_2FC=-2.92$, Figure 4D). *PSMA8* was not expressed in BOS (n=7) or control (n=7) fibroblasts, with normalized read counts of 0 in all samples, and a read count of 1 in one BOS fibroblast sample (Supplemental Figure 14G).

Truncating *ASXL1* mutations disrupt canonical and non-canonical Wnt signaling

Through integration of these data, we identified dysregulation of the canonical Wnt pathway (Figure 5A) in gene set enrichment analysis of RNA-seq (Figure 2E) and DNA methylation studies (Figure 4B), driven by a consistent pattern of canonical Wnt/β-catenin

pathway upregulation in the RNA-seq DEGs (Supplemental Table 26). Briefly, we identified upregulation of Wnt ligands: *WNT1* (log_2FC=0.87), *WNT7A* (log_2FC=0.97), and *WNT10B* (log_2FC=0.53) and upregulation of Wnt ligand receptor, *Frizzled* receptor *FZD3* (log_2FC=0.87).

Western blot quantification of representative BOS fibroblasts (n=5) and control (n=5) fibroblasts identified no significant differences in two key proteins that are typically regulated through spatial distribution, VANGL2 and β-Catenin, using bulk whole cell lysate (Figure 5B and 5C). Using a commercial Wnt antibody kit, we identified a fold increase of 1.5x for AXIN1, 2.8x for AXIN2, 3.5x for DVL2 and 1.5x for DVL3 averaged across BOS patient samples compared to controls (Figure 5C). While the ASXL1, histone marks, VANGL2, β-Catenin and β-actin levels were consistent between BOS samples, Pt3 and Pt4 exhibited control-like levels of AXIN2, DVL2 and, to some extent, DVL3.

RNA-seq and DNA methylation studies identified aberrant upregulation and hypomethylation of Wnt signaling co-receptors *LRP5* (Figure 5D-5F) and *LRP6* (Figure 5G-5I). We identified significant transcriptional upregulation of LRP5 (log2FC=1.64, p_{adj} =3.58x10^{-9}, Figure 5D and 5E) and LRP6 (log2FC=1.63, p_{adj} =1.17x10^{-12}, Figure 5G and 5H), 4 hypomethylated DNAm sites for *LRP5* (Δβ -3.5% to -8.0%, FDR<0.05) (Figure 5F), 2 of which reside in a CpG island, and 2 hypomethylated DNAm sites for *LRP6* (Δβ -2.7% to -4.0%, FDR<0.05), both of which reside in a CpG island (Figure 5I).

We also identified transcriptional upregulation of *AXIN2* (log_2FC=0.95) and downregulation of *GSK3B* (log_2FC=-0.28), consistent with canonical Wnt signaling activation. Endogenous *AXIN2* mRNA and protein expression is directly induced by Wnt pathway activation (62, 63) and used as a proxy reporter for Wnt pathway signaling. Furthermore, in BOS patient samples, the Wnt pathway transcription factors, *TCF7* (log_2FC=0.81) and *LEF1* (log_2FC=0.86) are both significantly transcriptionally upregulated.

Multi-omics identifies altered epigenetic profile in *VANGL2*, a non-canonical Wnt signaling gene, in BOS

VANGL2 first came to our attention as one of the most highly overexpressed DEGs in BOS blood and fibroblast RNA-seq data (Figure 2G, Supplemental Figures 15A and 15B). Integration of RNA-seq, ATAC-seq and DNAm data again identified *VANGL2* as differentially regulated in all datasets (Figure 3C and 4A). In BOS blood samples, we observed VANGL2 transcriptional upregulation coupled with hypomethylation (Δβ= -7.6%) at the TSS of VANGL2 CpG site cg17024258 (Figure 5J) and an inverse relationship between hypermethylation and transcriptional upregulation in individual samples (Supplemental Figure 15C). The 5' UTR of VANGL2 showed a 2.3-fold increase in chromatin accessibility by ATAC-seq (Figure 5K).

These findings were supported by differential gene expression of VANGL2 in BOS patients versus control samples. Cross-tissue RNA-seq integration (Figure 2G) showed that VANGL2 was significantly overexpressed in both BOS patient blood (log2FC=3.8, Figure 5L) and in fibroblasts (log2FC=2.55, Figure 5M).

Visualization of ATAC-seq data in IGV identified a clear increase in reads for BOS patients at the *VANGL2* TSS, representing more open chromatin (Figure 5N). Similarly, CUT&RUN for H3K4me3, an transcription-activating histone mark, showed significantly stronger H3K4me3 binding at the *VANGL2* TSS, for BOS compared to controls (Figure 5O). *ASXL1* has been previously shown to affect histone modifications, specifically H3K4me3, H3K27me3 and H2AK119ub, and our data further corroborates that truncating mutations in *ASXL1* result in loss of its gene repressive functions.

DISCUSSION

We utilized a multi-omics approach to profile primary BOS patient samples. For the first time, we directly link *ASXL1* mutations to activation of the canonical and the non-canonical Wnt-signaling pathway, namely the planar cell polarity (PCP) pathway. Both pathways are essential in

developmental patterning. The PCP pathway defines cell polarity and is essential to morphogenesis and diverse cellular processes (64). The data demonstrate that upregulation of Wnt pathways in BOS samples can be attributed to disruption of the epigenetic landscape ultimately resulting in transcriptomic dysregulation.

Most of the studies on human ASXL1 function are in the context of myeloid leukemia and propose that truncating *ASXL1* mutations result in haploinsufficiency (11, 36), dominant negative, or gain-of-function effects (31, 37, 38). In some reports, in vivo deletion of ASXL1 led to mild phenotypes of myeloid and lymphoid cell frequencies (7) while, in other reports, ASXL1 knockout mice had systemic developmental defects and MDS-like presentation suggesting a loss of function effect particularly in hematopoietic progenitor cells (11, 36). However, most ASXL1 mutations identified in human myeloid malignancies and in BOS do not harbor a deletion and, instead, harbor C-terminal nonsense or frameshift mutations. These mutations are hypothesized to escape nonsense-mediated decay and may potentially have a dominant-negative or gain-of-function effect (31). Our findings of comparable ASXL1 transcript and protein expression between BOS and control samples (Figures 1D, 2A, 2B, Supplemental Figure 2) are consistent with this hypothesis and show no evidence of degradation or nonsense mediated decay. The dysregulation observed in BOS may be a result of the combination of haploinsufficiency of the full-length transcript and translation of a short and non-functional protein that results in mistargeting of ASXL1 functions. Furthermore, developmental context may also play a role. This hypothesis is supported by iPSC studies conducted by Matheus et al. (9).

We also found comparable levels of wild type and pathogenic transcripts in BOS patients. This adds further evidence to existing literature that nonsense mediated decay and haploinsufficiency do not play a role in BOS pathogenesis (37, 65) which is, instead, mediated through mis-expression and impact, potentially through gain of function, of a truncated ASXL1 protein.

High-penetrance mutations in severe monogenic disorders supersede effects of age, sex and genetic background in molecular assays.

Although there is strong tissue-specific gene expression (66), we propose that the high-penetrance effect of truncating *ASXL1* mutations results in a set of dysregulated genes across tissues. The 25 common DEGs across BOS blood and fibroblast data support the overarching hypothesis that truncating *ASXL1* mutations exert a strong tissue-independent effect across tissues that have *ASXL1* expression. The functions of these key genes likely drive BOS pathophysiology and targeting these genes may provide a systemic treatment for BOS.

Some key challenges to the study of rare disease are the heterogeneity of ages at sample collection and diverse genetic background of patients. Controlling for age-specific effects and genetic background are important but would require statistical power that is near impossible with fewer than 100 patients reported worldwide. The control individuals for DNA methylation were matched for age- and sex- specific effects, while ATAC-seq and RNA-seq controls were matched for sex and genetic background effects. Integration between ATAC-seq, RNA-seq and DNA methylation data, and the identification of common dysregulated genes suggests that the role of truncating *ASXL1* mutations supersedes the effects of age and genetic background.

Integration of ATAC-seq and RNA-seq identified seven genes that were commonly dysregulated (Table 1). We tested these genes specifically for age-specific effects since that was a variable we were unable to sufficiently match given the young age of the BOS patient cohort, and restricted access to samples from healthy young children who do not require procedures. In our ATAC-seq and RNA-seq assays, we primarily used related parental controls to account for genetic variation in our population. The seven genes that were commonly dysregulated in our ATAC-seq and RNA-seq integration (Table 1), were all tested as part of a larger study by Lee et al. (67) through transcriptome analysis to classify human genes based on age-specific differential expression analysis. None of these genes showed an age-specific signature. These seven genes have important functions in body patterning and organogenesis, nervous system development

and ubiquitination regulation. While this does not rule out age-specific differences in potential interacting proteins, it suggests that truncating *ASXL1* effects are not significantly impacted by age.

ASXL1 represses canonical and non-canonical Wnt Signaling in normal development

One of the major findings in this study is the link of *ASXL1* mutations and the activation of the canonical and non-canonical Wnt-signaling pathways. The canonical Wnt signaling pathway plays an important role in embryonic development, stem cell maintenance, and differentiation of cells in adults and is highly conserved across species (68). The Wnt signaling pathway is under complex regulation and functions in context-specific manners, dependent on the receptors present on the cell membrane and Wnt ligand-receptor interactions at the time of pathway activation (69).

The molecular mechanisms and specific developmental stages of the interactions between the canonical and non-canonical Wnt pathways are not well elucidated. In the absence of Wnt signaling, β-catenin is degraded by the 26S proteasome, which is composed of two subcomplexes, the 20S proteasome and the regulatory particle (70), (71) (Figure 5A). PSMA8 is a subunit of the 20S proteasome, and hypermethylation and transcriptional downregulation of *PSMA8* in BOS patient samples (Figure 4C and 4D), suggests downregulation of the 26S proteasome-mediated degradation of β-catenin in BOS patient tissues (70). While PSMA8 is involved in numerous pathways within the cell, given the context of the many other Wnt signaling pathway genes that were identified as differentially regulated and differentially expressed (Supplemental Table 26), the hypermethylation and transcriptional downregulation of PSMA8 supports our findings of aberrant Wnt activation in RNA-seq (Figure 2E) and DNA methylation studies (Figure 4B) of BOS.

The "β-catenin destruction complex" consists of AXIN1, AXIN2, Dishevelled1/2/3 (DVL1, DVL2, DVL3), GSK3B and Adenomatous polyposis coli (APC). We identified increased protein

levels of AXIN1, AXIN2, DVL2, and DVL3 in BOS patient fibroblast samples. Pt3 and Pt4 exhibited control-like levels of AXIN2, DVL2 and, to some extent, DVL3. These two patients have truncating mutations within close proximity; at amino acid 635 and 642 respectively. This may point to a location specific effect of ASXL1 mutations, although more work is needed to elucidate this. BOS is a heterogeneous disorder and patient specific factors such as sex and age, or environmental effects may result in differential gene regulation. Pt3 and Pt4 are male BOS patients, while Pt2, Pt14 and Pt15 whom are female BOS patients have much higher levels of Wnt pathway proteins. No significant difference was identified between male and female control samples. Thus, this may point to sex-linked differential effects of truncating ASXL1 mutations on Wnt pathway protein expression, and would benefit from further study and replication in increased number of patient samples.

Western blot did not identify a difference in total whole cell β-catenin or VANGL2 levels between BOS and control fibroblasts (Figure 5B, 5C). These two genes are both post-translationally regulated, which may ultimately drive phenotype effects. More work is needed to elucidate the role of cellular localization of canonical and non-canonical Wnt proteins, and the role they play in BOS pathogenesis.

β-catenin localization is important in identifying activation of the Wnt signaling pathway. In the Wnt-active state, the "β-catenin destruction complex" is dissociated and culminates in nuclear translocation of β-catenin (43–45) (Figure 5A). This nuclear β-catenin binds to the TCF and LEF families, and initiates transcription of Wnt pathway targets (72, 73). *TCF7*, upregulated in BOS samples, is an important regulator of self-renewal and differentiation in multipotential hematopoietic cell lines (74), which could lend insight to the pathogenesis of myeloid cancers with truncating *ASXL1* mutations.

In contrast, the non-canonical pathways, including the PCP pathway which defines cell polarity and migration, are characterized by their β-catenin-independent regulation of crucial events during embryonic development (75). However, experiments that indicate their binary

utilization may be model-system and context-specific (48). Given the complex interplay and cross-talk at almost every level of the Wnt signaling pathways that we are just beginning to unravel, van Amerongen & Nusse suggest moving towards a more integrated view rather than the outdated binary classification (48).

Dysregulation of the Wnt signaling pathway identified in BOS samples may explain phenotypic presentations in BOS patients.

Wnt signaling plays a key role in hair growth and development of hair follicles. In particular, *WNT10B*, which is transcriptionally upregulated in BOS samples, promotes differentiation of primary skin epithelial cells towards the hair shaft in mice and elongation of the hair shaft in isolated rabbit whisker hair follicles (76–78). Intriguingly, many providers and parents have noted excessive hypertrichosis with rapidly growing hair and nails in BOS patients (25). It is possible that aberrant activation of Wnt signaling may play an important role here in BOS patient pathophysiology.

Other significant Wnt signaling DEGs in our datasets include *WNT1*, important in regulating cell fate and patterning during embryogenesis, and *WNT7A*, a key embryonic dorsal vs ventral patterning gene and a key regulator of normal neural stem cell renewal, proliferation, and differentiation. *WNT7A* activates the PCP pathway and *Wnt7a* overexpression has been shown to induce *Vangl2* overexpression and impair neurulation in mouse neural stem cells through aberrant Vangl2 polarized distribution (79, 80).

Collectively, our epigenomic, transcriptional and protein data of the Wnt signaling pathways corroborate a distinct and consistent activation of canonical Wnt signaling in BOS samples and may lend insight to patient phenotypes.

Upregulation of non-canonical Wnt signaling gene *VANGL2* in BOS drives clinical phenotypes.

VANGL2 was one of the most highly dysregulated genes in all our datasets with a 9-fold increase in gene expression occurring via epigenetic dysregulation (Figures 5J - 5O). VANGL2 is thought to regulate Wnt protein distribution (81) and, in its non-canonical role, has been shown to play critical roles in neurulation, cardiac development, kidney-branching morphogenesis and regulation of hematopoiesis (49, 82–84). The PCP pathway is a highly conserved non-canonical Wnt signaling pathway important in establishing and maintaining polarity during morphogenesis. While we identified no significant difference in total VANGL2 protein at the whole cell level between BOS and control fibroblasts (Figures 5B, 5C), like β-catenin, VANGL2 function is strongly dependent upon cellular localization. The asymmetric localization on the plasma membrane of VANGL2 is needed for signal transduction, and subsequent polarization and organization of cells (85). The PCP pathway is also crucial for neural tube closure (86) and it has been suggested that the gradient of Wnt activity helps establish VANGL2 polarity in the neural plate during neurulation (87), with canonical Wnt signaling required for neural crest induction, and non-canonical Wnt pathway required for neural crest migration (88).

Knockout and loss-of-function studies in *Vangl2* identified significant reduction in spine density and dendritic branching in primary culture rat hippocampal neurons (49). In humans, homozygous mutations in *VANGL2* are embryonic lethal and cause craniorachischisis, a very severe neural tube defect encompassing anencephaly and bony defects of the spine, in mice (89) whereas heterozygous *VANGL2* mutations are embryonic lethal and detected in miscarried human fetuses with severe cranial neural-tube defects (90). Neural crest cells contribute to nervous system and craniofacial development, and are critical for cardiac outflow septation and alignment (91). Perhaps not surprisingly, *Vangl2* knockout mice exhibit cardiac outflow tract malformations and septal defects (82), as do BOS patients (25). These findings suggest that the severe neural phenotype, distinctive craniofacial features, and cardiac defects of patients with BOS (25) may be due, at least in part, to the dysregulation of *VANGL2* and downstream effects on neural crest migration.

Although the interplay between the canonical Wnt and non-canonical Wnt pathways is not well understood, recent literature has suggested that these pathways exert reciprocal pathway inhibition through competition for a common downstream coreceptor *FZD* (75, 92), most evident during tissue regeneration and development (93, 94). The asymmetric localization of *FZD3* required for proper function is dependent on anchoring by *VANGL2* through physical interaction of the two proteins (95). We identified upregulation of *FZD3*, which regulates establishment of the non-canonical Wnt/PCP pathway and is involved in neural crest cell migration and neural tube closure (96, 97). These results are supported by molecular characterization of truncating *ASXL1* mutations conducted in iPSCs (9).

A limitation of this study is that BOS pathophysiology is shaped by cellular context and developmental stage and our study is focused on differentiated cell types. Cellular and developmental context can drastically affect the molecular effects of epigenetic modifiers such as *ASXL1*. The effects of *ASXL1* begin in early embryogenesis (98) so embryonic stem cells would be the ideal model to recapture cell types where *ASXL1* is maximally impacting progenitors of clinical phenotypes. These multi-omics approaches will benefit from being performed in patient-derived stem-cell models and through samples generated with introduction of truncating *ASXL1* mutations using DNA- editing systems. Moving into stem-cell models will yield additional insights into the role of *ASXL1* in stem cell homeostasis and differentiation.

In conclusion, we present a comprehensive multi-omics analysis of BOS using primary patient samples. This study encompasses the largest omics study of patients with BOS, a very rare genetic disorder. We present the first analyses of RNA-seq and ATAC-seq conducted on primary BOS patient samples. Through DNAm, identifying binding proteins, deciphering chromatin accessibility, and gene expression analysis, we add to growing literature on *ASXL1* and the pathogenesis of ASXL1 truncating mutations. Our integrated methods identified dysregulation of key transcripts such as *VANGL2* through direct chromatin modifications. This suggests that physiological levels of truncating *ASXL1* mutation lead to loss of the repressive

function of *ASXL1*. Importantly, pathways that are dysregulated across multiple assays are involved in neural development, which shed light on the severe intellectual and neural features in BOS patients, and Wnt/β-catenin and non-canonical Wnt PCP pathways which represent key, drug-targetable pathways. Our findings have major implications for identifying potential therapeutics for diseases harboring *ASXL1* mutations.

METHODS

Cell Culture. Patient-derived fibroblast cell lines were grown in DMEM (Gibco™, #11-995-073), 10% FBS, 1% Non-essential Amino Acid (100X, Gibco™, 11140-050) and 1% PenStrep at 37℃ in 5% CO_2 incubators.

Western Blots. Whole cell lysate was extracted with Cell Lysis Buffer (10X, Cell Signaling #9803S), cytoplasmic and nuclear extractions using the Thermo Scientific CE/NER Kit (#78833), and histones were extracted as per established protocol (99). See Supplemental Methods.

RNA-sequencing. Fibroblasts were grown to 80-90% confluency in T75 flasks before total RNA extraction via RNeasy Plus Mini Kit (Qiagen, #74136). Blood samples were first treated with QIAseq FastSelect −Globin (Qiagen, #334376). All samples were then prepared with QIAseq FastSelect −rRNA HMR (Qiagen, #334386) and Illumina Truseq® Stranded Total RNA Library Prep Gold (Illumina, 20020599), before sequencing to a minimum of 30 million paired end 150bp reads per sample. See Supplemental Methods.

ATAC-Seq. Fibroblast lines were cultured to 80-90% confluency in T75 flasks and 50,000 freshly isolated cells per line were treated with Tn5 transposase as per established protocol (100). Libraries were sequenced to a minimum of 40 million paired-end reads per sample with 75bp length. See Supplemental Methods.

CUT&RUN. CUT&RUN libraries were prepared with the established CUT&RUN Assay Kit (Cell Signaling, #86652S). See Supplemental Methods. Samples were analyzed using the established NF-Core CUT&RUN analysis pipeline(101).

DNA methylation.

See Supplemental Methods.

RT-qPCR. RT-qPCR was conducted using TaqPath™ 1-Step RT-qPCR Master Mix, CG (Applied Biosystems, A15300) according to protocol (Document #100020171, Rev 1.00) on QuantStudio™ 3. See Supplemental Methods for further information.

STATISTICS

Statistics. RNA-seq, ATAC-seq, and CUT&RUN reads were aligned to the human genome (hg38) and featureCounts (v1.6.5) was used to generate count matrices for genes or chromatin regions. DESeq2 (v1.24.0), which internally normalizes sample library size and utilizes the negative binomial distribution for testing, was used to identify differentially expressed genes (RNA-seq) or differentially accessible chromatin regions (ATAC-seq, CUT&RUN) after adjusting for sample sex, which was identified as a covariate to adjust for through PCAs generated based on the top 500 most variably expressed genes. Genes or regions were identified as significant if Benjamini-Hochberg adjusted p-values (padj) <0.05. We further filtered for highly dysregulated significant genes or regions using an abs(log2FoldChange)≥0.58, corresponding to an abs(FoldChange)≥1.5 with reference to control samples. Gene ontology over-enrichment tests were completed using clusterProfiler v3.12.0 by submitting differentially expressed genes against all genes from the Gencode hg38 annotation, version 31. Gene ontologies were classified as significantly enriched when padj (Benjamini-Hochberg) < 0.05 (hypergeometric test).

DNAm beta (β) values were calculated using minfi (102), and differentially methylated sites were identified by running Limma regression modeling, while adjusting for the covariates of age, sex, and ethnicity. Our significance cut-offs were FDR<0.05 (Benjamini-Hochberg). We filtered for significantly methylated CpG sites with abs(Δβ)>0.10, where Δβ represents the difference in average DNAm (β) between BOS and controls. GREAT (60) was run on significant CpG sites to identify biological mechanisms that were dysregulated, filtering for gene ontologies with padj<0.05 for significance.

Study Approval. This project was approved by the UCLA IRB# 11-001087. In conjunction with Dr. Bianca Russell and the ASXL Biobank at the University of California, Los Angeles, written informed consent from participants and guardians were obtained for skin punch biopsies and blood samples. Deep phenotyping and review of medical records was also collected.

Author Contributions.

VA, ZA and IL designed and conceptualized the study and wrote the paper. IL, MS and AW performed data generation and transcriptomic and epigenomic data analysis for patient-derived samples. BR and REACH coordinated sample collection. ZA and RW performed data generation and analysis of DNA methylation data. All authors contributed to the writing of and the editing of the manuscript.

Acknowledgements. This work was supported by the following funding sources awarded to V.A.A.: NIH DP5OD024579 and the ASXL Research Related Endowment Pilot Grant (2020-2022). IL was supported by NIH T32 GM008042. ZA and RW are supported by the ASXL Research Related Endowment Pilot Grant (2020-2022), the Canadian Institutes of Health Research (CIHR) grants (IGH-155182 and MOP-126054), and the Ontario Brain Institute (province of Ontario Neurodevelopmental Disorders (POND) network (IDS11-02)) grants to RW. We would like to acknowledge the families and patients who participated in this study and donated their time and efforts to make this possible. We would also like to acknowledge Elisabeth McGee for her work in coordinating sample collection and The California Center for Rare Disease for their support and building of critical infrastructure for these studies. Some of the figures in this paper were created with BioRender.com.

Public Data Sets.

https://portal.gdc.cancer.gov/projects/TCGA-LAML.

Conflict of interest statement.

The authors have declared that no conflict of interest exists.

REFERENCES

1. Fisher CL, et al. A human homolog of Additional sex combs, ADDITIONAL SEX COMBS-LIKE 1, maps to chromosome 20q11. *Gene* 2003;306:115–126.

2. Aravind L, Iyer LM. The HARE-HTH and associated domains: novel modules in the coordination of epigenetic DNA and protein modifications. *Cell Cycle* 2012;11(1):119–131.

3. Katoh M. Functional proteomics of the epigenetic regulators ASXL1, ASXL2 and ASXL3: a convergence of proteomics and epigenetics for translational medicine. *Expert Rev. Proteomics* 2015;12(3):317–328.

4. Jain K, et al. Characterization of the plant homeodomain (PHD) reader family for their histone tail interactions. *Epigenetics Chromatin* 2020;13(1):3.

5. Sanchez R, Zhou M-M. The PHD finger: a versatile epigenome reader. *Trends Biochem. Sci.* 2011;36(7):364–372.

6. Schuettengruber B, et al. Genome Regulation by Polycomb and Trithorax: 70 Years and Counting. *Cell* 2017;171(1):34–57.

7. Fisher CL, et al. Additional sex combs-like 1 belongs to the enhancer of trithorax and polycomb group and genetically interacts with Cbx2 in mice. *Dev. Biol.* 2010;337(1):9–15.

8. Sinclair DA, et al. Genetic analysis of the additional sex combs locus of Drosophila melanogaster. *Genetics* 1992;130(4):817–825.

9. Matheus F, et al. Pathological ASXL1 Mutations and Protein Variants Impair Neural Crest Development. *Stem Cell Reports* 2019;12(5):861–868.

10. McGinley AL, et al. Additional sex combs-like family genes are required for normal cardiovascular development. *Genesis* 2014;52(7):671–686.

11. Abdel-Wahab O, et al. Deletion of Asxl1 results in myelodysplasia and severe developmental defects in vivo. *J. Exp. Med.* 2013;210(12):2641–2659.

12. Yamato G, et al. ASXL2mutations are frequently found in pediatric AML patients with t(8;21)/RUNX1-RUNX1T1and associated with a better prognosis. *Genes Chromosomes Cancer* 2017;56(5):382–393.

13. Pereira JD, et al. Ezh2, the histone methyltransferase of PRC2, regulates the balance between self-renewal and differentiation in the cerebral cortex. *Proc. Natl. Acad. Sci. U. S. A.* 2010;107(36):15957–15962.

14. Sahtoe DD, et al. BAP1/ASXL1 recruitment and activation for H2A deubiquitination. *Nat. Commun.* 2016;7:10292.

15. Inoue D, et al. The stability of epigenetic factor ASXL1 is regulated through ubiquitination and USP7-mediated deubiquitination. *Leukemia* 2015;29(11):2257–2260.

16. Rothberg JLM, et al. Mtf2-PRC2 control of canonical Wnt signaling is required for definitive erythropoiesis. *Cell Discov* 2018;4:21.

17. Chen J, et al. The microtubule-associated protein PRC1 promotes early recurrence of hepatocellular carcinoma in association with the Wnt/β-catenin signalling pathway. *Gut* 2016;65(9):1522–1534.

18. Asada S, et al. Mutant ASXL1 cooperates with BAP1 to promote myeloid leukaemogenesis. *Nature Communications* 2018;9(1). doi:10.1038/s41467-018-05085-9

19. Asada S, Kitamura T. Aberrant histone modifications induced by mutant ASXL1 in myeloid neoplasms. *Int. J. Hematol.* 2019;110(2):179–186.

20. Kweon S-M, et al. An Adversarial DNA N6-Methyladenine-Sensor Network Preserves Polycomb Silencing. *Mol. Cell* 2019;74(6):1138–1147.e6.

21. Srivastava A, McGrath B, Bielas SL. Histone H2A Monoubiquitination in Neurodevelopmental Disorders. *Trends in Genetics* 2017;33(8):566–578.

22. Srivastava A, et al. De novo dominant ASXL3 mutations alter H2A deubiquitination and transcription in Bainbridge–Ropers syndrome. *Hum. Mol. Genet.* 2015;25(3):597–608.

23. Bainbridge MN, et al. De novo truncating mutations in ASXL3 are associated with a novel clinical phenotype with similarities to Bohring-Opitz syndrome. *Genome Med.* 2013;5(2):11.

24. Fang X, et al. Asxl1 C-terminal mutation perturbs neutrophil differentiation in zebrafish. *Leukemia* 2021;35(8):2299–2310.

25. Russell B, Tan W-H, Graham JM Jr. Bohring-Opitz Syndrome. In: Adam MP et al eds. *GeneReviews®*. Seattle (WA): University of Washington, Seattle; 2018:

26. Hoischen A, et al. De novo nonsense mutations in ASXL1 cause Bohring-Opitz syndrome. *Nat. Genet.* 2011;43(8):729–731.

27. Shashi V, et al. De Novo Truncating Variants in ASXL2 Are Associated with a Unique and Recognizable Clinical Phenotype. *Am. J. Hum. Genet.* 2016;99(4):991–999.

28. Russell B, Graham JM. Expanding our knowledge of conditions associated with the ASXL gene family. *Genome Med.* 2013;5(2):1–3.

29. Pratcorona M, et al. Acquired mutations in ASXL1 in acute myeloid leukemia: prevalence and prognostic value. *Haematologica* 2012;97(3):388–392.

30. Genovese G, et al. Clonal hematopoiesis and blood-cancer risk inferred from blood DNA sequence. *N. Engl. J. Med.* 2014;371(26):2477–2487.

31. Gelsi-Boyer V, et al. Mutations in ASXL1 are associated with poor prognosis across the spectrum of malignant myeloid diseases. *J. Hematol. Oncol.* 2012;5:12.

32. Micol J-B, Abdel-Wahab O. The Role of Additional Sex Combs-Like Proteins in Cancer. *Cold Spring Harb. Perspect. Med.* 2016;6(10). doi:10.1101/cshperspect.a026526

33. Dawoud AAZ, Tapper WJ, Cross NCP. Clonal myelopoiesis in the UK Biobank cohort: ASXL1 mutations are strongly associated with smoking. *Leukemia* 2020;34(10):2660–2672.

34. Jaiswal S, et al. Age-related clonal hematopoiesis associated with adverse outcomes. *N. Engl. J. Med.* 2014;371(26):2488–2498.

35. Nagase R, et al. Expression of mutant Asxl1 perturbs hematopoiesis and promotes susceptibility to leukemic transformation. *J. Exp. Med.* 2018;215(6):1729–1747.

36. Wang J, et al. Loss of Asxl1 leads to myelodysplastic syndrome-like disease in mice. *Blood* 2014;123(4):541–553.

37. Inoue D, et al. Truncation mutants of ASXL1 observed in myeloid malignancies are expressed at detectable protein levels. *Experimental Hematology* 2016;44(3):172–176.e1.

38. Yang H, et al. Gain of function of ASXL1 truncating protein in the pathogenesis of myeloid malignancies. *Blood* 2018;131(3):328–341.

39. Guo M, et al. Epigenetic heterogeneity in cancer. *Biomark Res* 2019;7:23.

40. Nusse R, Clevers H. Wnt/β-Catenin Signaling, Disease, and Emerging Therapeutic Modalities. *Cell* 2017;169(6):985–999.

41. Malhotra S, Kincade PW. Canonical Wnt pathway signaling suppresses VCAM-1 expression by marrow stromal and hematopoietic cells. *Exp. Hematol.* 2009;37(1):19–30.

42. Tamai K, et al. LDL-receptor-related proteins in Wnt signal transduction. *Nature* 2000;407(6803):530–535.

43. Wu D, Pan W. GSK3: a multifaceted kinase in Wnt signaling. *Trends Biochem. Sci.* 2010;35(3):161–

168.

44. Mao J, et al. Low-density lipoprotein receptor-related protein-5 binds to Axin and regulates the canonical Wnt signaling pathway. *Mol. Cell* 2001;7(4):801–809.

45. Kim S-E, et al. Wnt stabilization of β-catenin reveals principles for morphogen receptor-scaffold assemblies. *Science* 2013;340(6134):867–870.

46. Wang B, et al. Targeting Wnt/β-catenin signaling for cancer immunotherapy. *Trends Pharmacol. Sci.* 2018;39(7):648–658.

47. Gajos-Michniewicz A, Czyz M. WNT signaling in melanoma. *Int. J. Mol. Sci.* 2020;21(14):4852.

48. van Amerongen R, Nusse R. Towards an integrated view of Wnt signaling in development. *Development* 2009;136(19):3205–3214.

49. Hagiwara A, et al. The planar cell polarity protein Vangl2 bidirectionally regulates dendritic branching in cultured hippocampal neurons. *Mol. Brain* 2014;7:79.

50. Russell BE, et al. Clinical findings in 39 individuals with Bohring-Opitz syndrome from a global patient-driven registry with implications for tumor surveillance and recurrence risk. *Am. J. Med. Genet. A* 2023;191(4):1050–1058.

51. Awamleh Z, et al. DNA methylation signature associated with Bohring-Opitz syndrome: a new tool for functional classification of variants in ASXL genes. *Eur. J. Hum. Genet.* [published online ahead of print: April 1, 2022]; doi:10.1038/s41431-022-01083-0

52. Buenrostro JD, et al. ATAC-seq: A Method for Assaying Chromatin Accessibility Genome-Wide. *Curr. Protoc. Mol. Biol.* 2015;109:21.29.1–21.29.9.

53. Skene PJ, Henikoff JG, Henikoff S. Targeted in situ genome-wide profiling with high efficiency for low cell numbers. *Nat. Protoc.* 2018;13(5):1006–1019.

54. Balasubramani A, et al. Cancer-associated ASXL1 mutations may act as gain-of-function mutations of the ASXL1–BAP1 complex. *Nat. Commun.* 2015;6(1):1–15.

55. Abdel-Wahab O, et al. ASXL1 mutations promote myeloid transformation through loss of PRC2-mediated gene repression. *Cancer Cell* 2012;22(2):180–193.

56. Russell B, et al. Clinical management of patients with ASXL1 mutations and Bohring-Opitz syndrome, emphasizing the need for Wilms tumor surveillance. *Am. J. Med. Genet. A* 2015;167A(9):2122–2131.

57. Heinz S, et al. Simple combinations of lineage-determining transcription factors prime cis-regulatory elements required for macrophage and B cell identities. *Mol. Cell* 2010;38(4):576–589.

58. Guo H, et al. DNA methylation and chromatin accessibility profiling of mouse and human fetal germ cells. *Cell Res.* 2017;27(2):165–183.

59. Yan F, et al. From reads to insight: a hitchhiker's guide to ATAC-seq data analysis. *Genome Biol.* 2020;21(1):22.

60. McLean CY, et al. GREAT improves functional interpretation of cis-regulatory regions. *Nat. Biotechnol.* 2010;28(5):495–501.

61. Yu G, et al. clusterProfiler: an R package for comparing biological themes among gene clusters. *OMICS* 2012;16(5):284–287.

62. Jho E-H, et al. Wnt/beta-catenin/Tcf signaling induces the transcription of Axin2, a negative regulator of the signaling pathway. *Mol. Cell. Biol.* 2002;22(4):1172–1183.

63. Lustig B, et al. Negative feedback loop of Wnt signaling through upregulation of conductin/axin2 in colorectal and liver tumors. *Mol. Cell. Biol.* 2002;22(4):1184–1193.

64. Jones C, Chen P. Planar cell polarity signaling in vertebrates. *Bioessays* 2007;29(2):120–132.

65. Inoue D, et al. Myelodysplastic syndromes are induced by histone methylation–altering ASXL1 mutations. *J. Clin. Invest.* 2013;123(11):4627–4640.

66. Dezso Z, et al. A comprehensive functional analysis of tissue specificity of human gene expression. *BMC Biol.* 2008;6:49.

67. Lee G, Lee M. Classification of Genes Based on Age-Related Differential Expression in Breast Cancer. *Genomics Inform.* 2017;15(4):156–161.

68. Kim JH, et al. Wnt signaling in bone formation and its therapeutic potential for bone diseases. *Ther. Adv. Musculoskelet. Dis.* 2013;5(1):13–31.

69. van Amerongen R, Mikels A, Nusse R. Alternative wnt signaling is initiated by distinct receptors. *Sci. Signal.* 2008;1(35):re9.

70. Park H-B, Kim J-W, Baek K-H. Regulation of Wnt Signaling through Ubiquitination and Deubiquitination in Cancers. *Int. J. Mol. Sci.* 2020;21(11). doi:10.3390/ijms21113904

71. Mao Y. Structure, Dynamics and Function of the 26S Proteasome. In: Harris JR, Marles-Wright J eds. *Macromolecular Protein Complexes III: Structure and Function*. Cham: Springer International Publishing; 2021:1–151

72. Rao TP, Kühl M. An updated overview on Wnt signaling pathways: a prelude for more. *Circ. Res.* 2010;106(12):1798–1806.

73. van de Wetering M, et al. The beta-catenin/TCF-4 complex imposes a crypt progenitor phenotype on colorectal cancer cells. *Cell* 2002;111(2):241–250.

74. Wu JQ, et al. Tcf7 is an important regulator of the switch of self-renewal and differentiation in a multipotential hematopoietic cell line. *PLoS Genet.* 2012;8(3):e1002565.

75. Grumolato L, et al. Canonical and noncanonical Wnts use a common mechanism to activate

completely unrelated coreceptors. *Genes Dev.* 2010;24(22):2517–2530.

76. Montcouquiol M, et al. Identification of Vangl2 and Scrb1 as planar polarity genes in mammals. *Nature* 2003;423(6936):173–177.

77. Cetera M, et al. Planar cell polarity-dependent and independent functions in the emergence of tissue-scale hair follicle patterns. *Dev. Biol.* 2017;428(1):188–203.

78. Wu Z, et al. Wnt10b promotes hair follicles growth and dermal papilla cells proliferation via Wnt/β-Catenin signaling pathway in Rex rabbits. *Biosci. Rep.* 2020;40(2). doi:10.1042/BSR20191248

79. Shariatmadari M, et al. Increased Wnt levels in the neural tube impair the function of adherens junctions during neurulation. *Mol. Cell. Neurosci.* 2005;30(3):437–451.

80. Le Grand F, et al. Wnt7a activates the planar cell polarity pathway to drive the symmetric expansion of satellite stem cells. *Cell Stem Cell* 2009;4(6):535–547.

81. Brunt L, et al. Vangl2 promotes the formation of long cytonemes to enable distant Wnt/β-catenin signaling. *Nat. Commun.* 2021;12(1):2058.

82. Ramsbottom SA, et al. Vangl2-regulated polarisation of second heart field-derived cells is required for outflow tract lengthening during cardiac development. *PLoS Genet.* 2014;10(12):e1004871.

83. Yates LL, et al. The planar cell polarity gene Vangl2 is required for mammalian kidney-branching morphogenesis and glomerular maturation. *Hum. Mol. Genet.* 2010;19(23):4663–4676.

84. Bouali S, et al. Vangl2 Promotes Hematopoietic Stem Cell Expansion. *Front Cell Dev Biol* 2022;10:760248.

85. Torban E, et al. Tissue, cellular and sub-cellular localization of the Vangl2 protein during embryonic development: effect of the Lp mutation. *Gene Expr. Patterns* 2007;7(3):346–354.

86. Ueno N, Greene NDE. Planar cell polarity genes and neural tube closure. *Birth Defects Res. C*

Embryo Today 2003;69(4):318–324.

87. Ossipova O, Kim K, Sokol SY. Planar polarization of Vangl2 in the vertebrate neural plate is controlled by Wnt and Myosin II signaling. *Biol. Open* 2015;4(6):722–730.

88. De Calisto J, et al. Essential role of non-canonical Wnt signalling in neural crest migration. *Development* 2005;132(11):2587–2597.

89. Torban E, et al. Independent mutations in mouse Vangl2 that cause neural tube defects in looptail mice impair interaction with members of the Dishevelled family. *J. Biol. Chem.* 2004;279(50):52703–52713.

90. Lei Y-P, et al. VANGL2 mutations in human cranial neural-tube defects. *N. Engl. J. Med.* 2010;362(23):2232–2235.

91. Kirby ML. Cellular and molecular contributions of the cardiac neural crest to cardiovascular development. *Trends Cardiovasc. Med.* 1993;3(1):18–23.

92. Corda G, Sala A. Non-canonical WNT/PCP signalling in cancer: Fzd6 takes centre stage. *Oncogenesis* 2017;6(7):e364.

93. van Amerongen R. Alternative Wnt pathways and receptors. *Cold Spring Harb. Perspect. Biol.* 2012;4(10). doi:10.1101/cshperspect.a007914

94. Angers S, Moon RT. Proximal events in Wnt signal transduction. *Nat. Rev. Mol. Cell Biol.* 2009;10(7):468–477.

95. Montcouquiol M, et al. Asymmetric localization of Vangl2 and Fz3 indicate novel mechanisms for planar cell polarity in mammals. *J. Neurosci.* 2006;26(19):5265–5275.

96. Hua ZL, et al. Frizzled3 is required for the development of multiple axon tracts in the mouse central nervous system. *Proc. Natl. Acad. Sci. U. S. A.* 2014;111(29):E3005–14.

97. Hua ZL, Smallwood PM, Nathans J. Frizzled3 controls axonal development in distinct populations of cranial and spinal motor neurons. *Elife* 2013;2:e01482.

98. Perez-Garcia V, et al. BAP1/ASXL complex modulation regulates epithelial-mesenchymal transition during trophoblast differentiation and invasion. *Elife* 2021;10. doi:10.7554/eLife.63254

99. Vogelauer M, et al. Stimulation of Histone Deacetylase Activity by Metabolites of Intermediary Metabolism*. *J. Biol. Chem.* 2012;287(38):32006–32016.

100. Corces MR, et al. An improved ATAC-seq protocol reduces background and enables interrogation of frozen tissues. *Nat. Methods* 2017;14(10):959–962.

101. Meers MP, et al. Improved CUT&RUN chromatin profiling tools. *Elife* 2019;8. doi:10.7554/eLife.46314

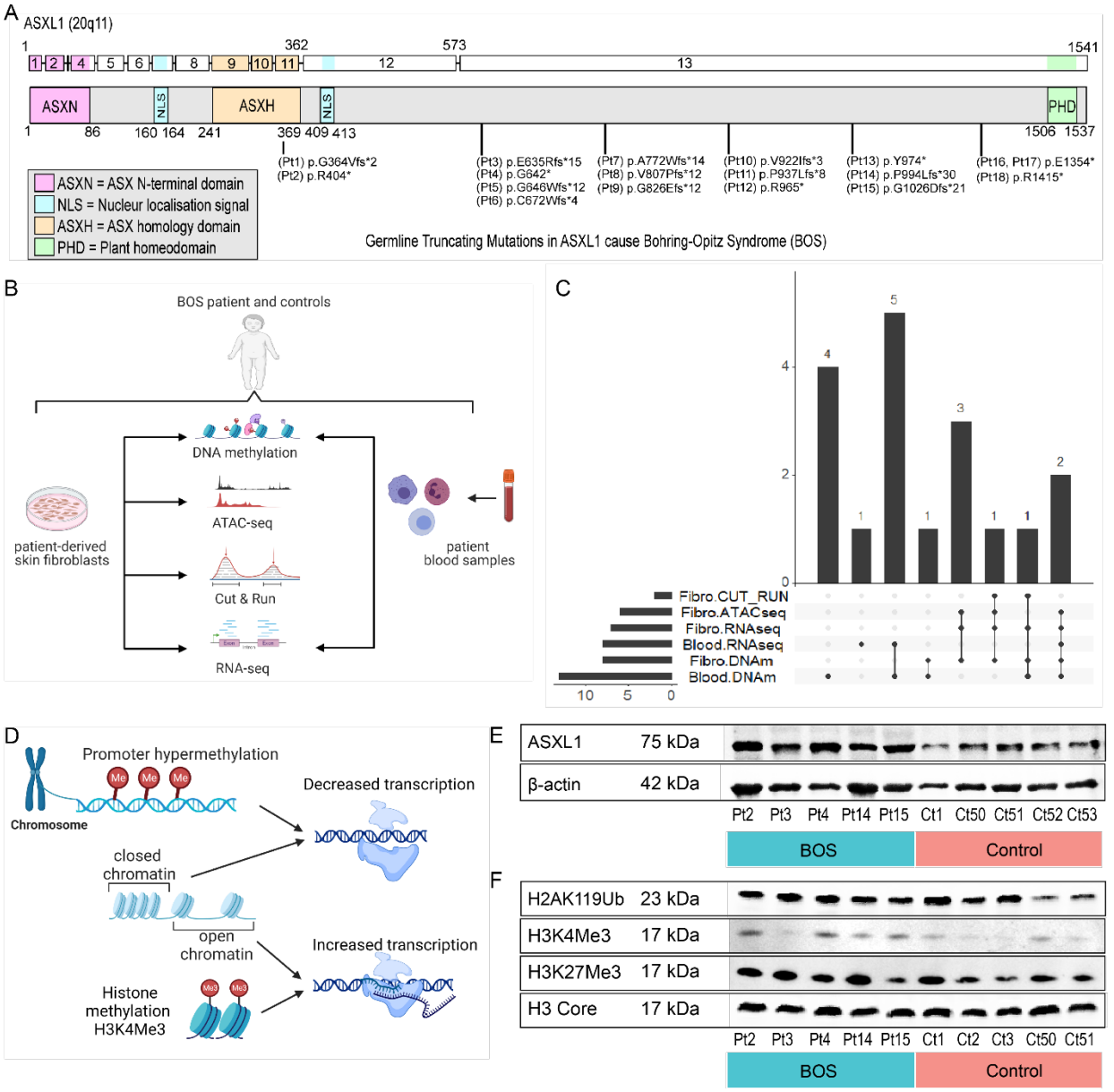

Figure 1. Multi-omics study design for Bohring-Opitz Syndrome (BOS) caused by pathogenic mutations in *ASXL1*. (A) Schematic representation of the ASXL1 transcript (ENST00000375687.10) and protein (GenBank: ASXL1; NM_015338.6; GRCh37), its functional domains, and mutations causing BOS. Mutations listed correspond to patients in this study and are tagged with a Pt identifier. **(B)** Peripheral blood and dermal fibroblasts were collected and underwent epigenomic assays for ATAC-seq, CUT&RUN, and global transcriptome analysis using RNA-seq. **(C)** Across the multi-omics assays and two specimen types we had 8/18 BOS samples with fibroblast assays, 14/18 with blood assays. 4/18 BOS patients had data from assays across both specimen types. (D) Promoter hypermethylation and closed chromatin, which can be examined with DNA methylation and ATAC-seq analysis respectively, are associated with decreased transcription while activating histone methylation such as H3K4Me3 at promoters and open chromatin are associated with increased transcription. Western blot for representative BOS (n=5) and representative control (n=5) fibroblast (E) whole cell lysate extracts shows no significant difference in total ASXL1 protein. This was repeated 3 times. (F) Fibroblast histone extracts showed no significant difference in H2AK119ub, H3K4me3 and H3K27me3. This was repeated 3 times.

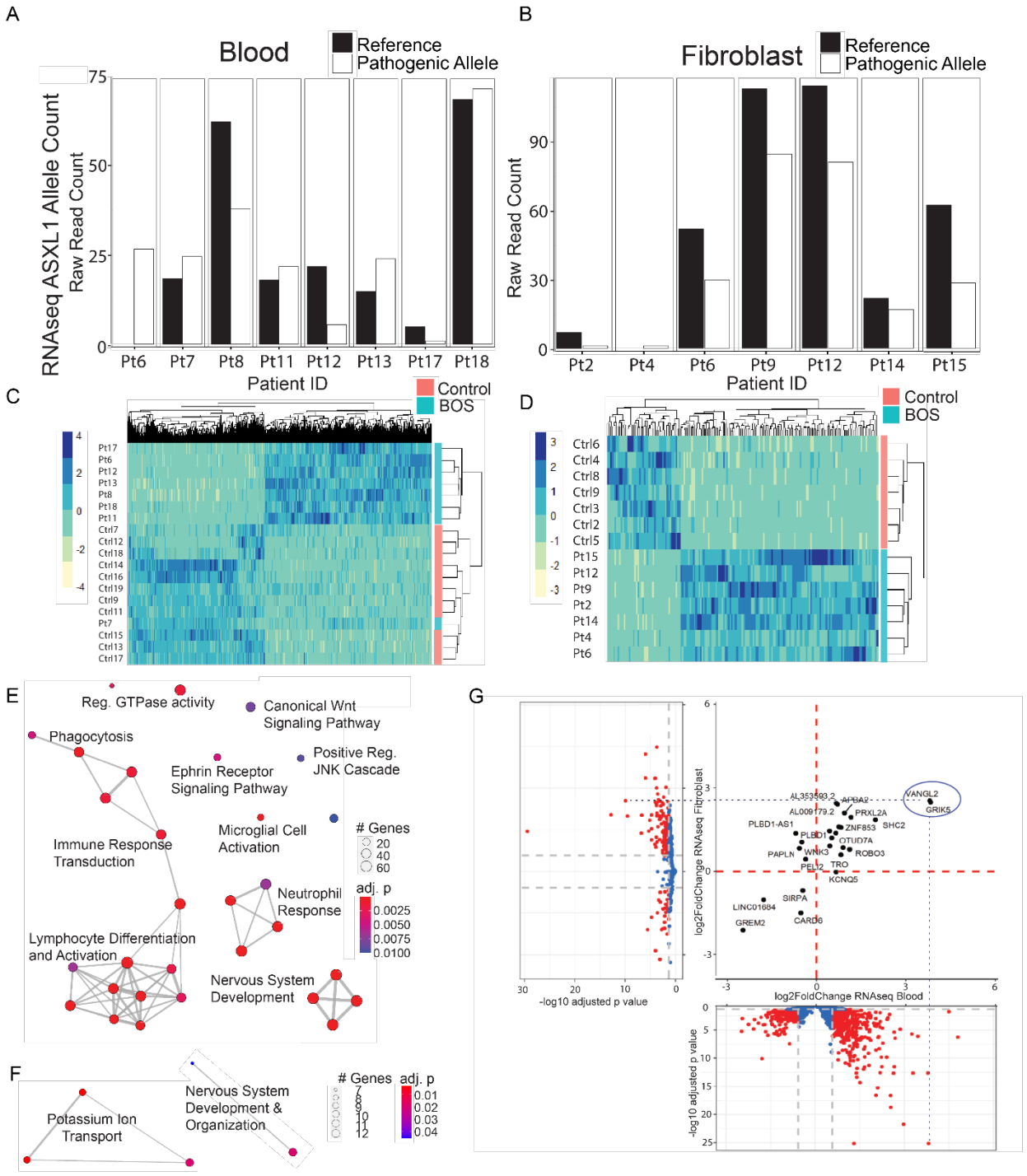

Figure 2: Pathogenic mutations in *ASXL1* cause tissue-specific and tissue-independent effects on gene expression. (A) RNA-seq raw read counts for the *ASXL1* reference allele (black) and pathogenic allele (white, with black outline) at each BOS patient's respective mutation in blood (n=8) and **(B)** fibroblast (n=7) samples. **(C)** RNA-seq heatmap of all significant DEGs with adjusted p<0.05 and $|\log_2 FC| \geq 0.58$ between BOS (blue, n=8) and control (pink, n=11) blood found 1097 DEGs with 590/1097 (53.8%) being more upregulated and **(D)** 155 DEGs between BOS (n=7) and control (n=7) fibroblasts, with 125/155 DEGs (80.6%) being more upregulated in BOS patients. **(E)** Blood RNA-seq gene ontology highlighted enrichment of genes related to

nervous system development and canonical Wnt signaling pathway. (F) Fibroblast RNA-seq gene ontology highlighted enrichment of genes related to nervous system development. **(G)** Volcano plots for BOS compared to control RNA-seq in blood (x-axis) and fibroblast (y-axis) identified a core subset of 25 shared dysregulated transcripts, with 21/25 DEGs (84%) dysregulated in the same direction.

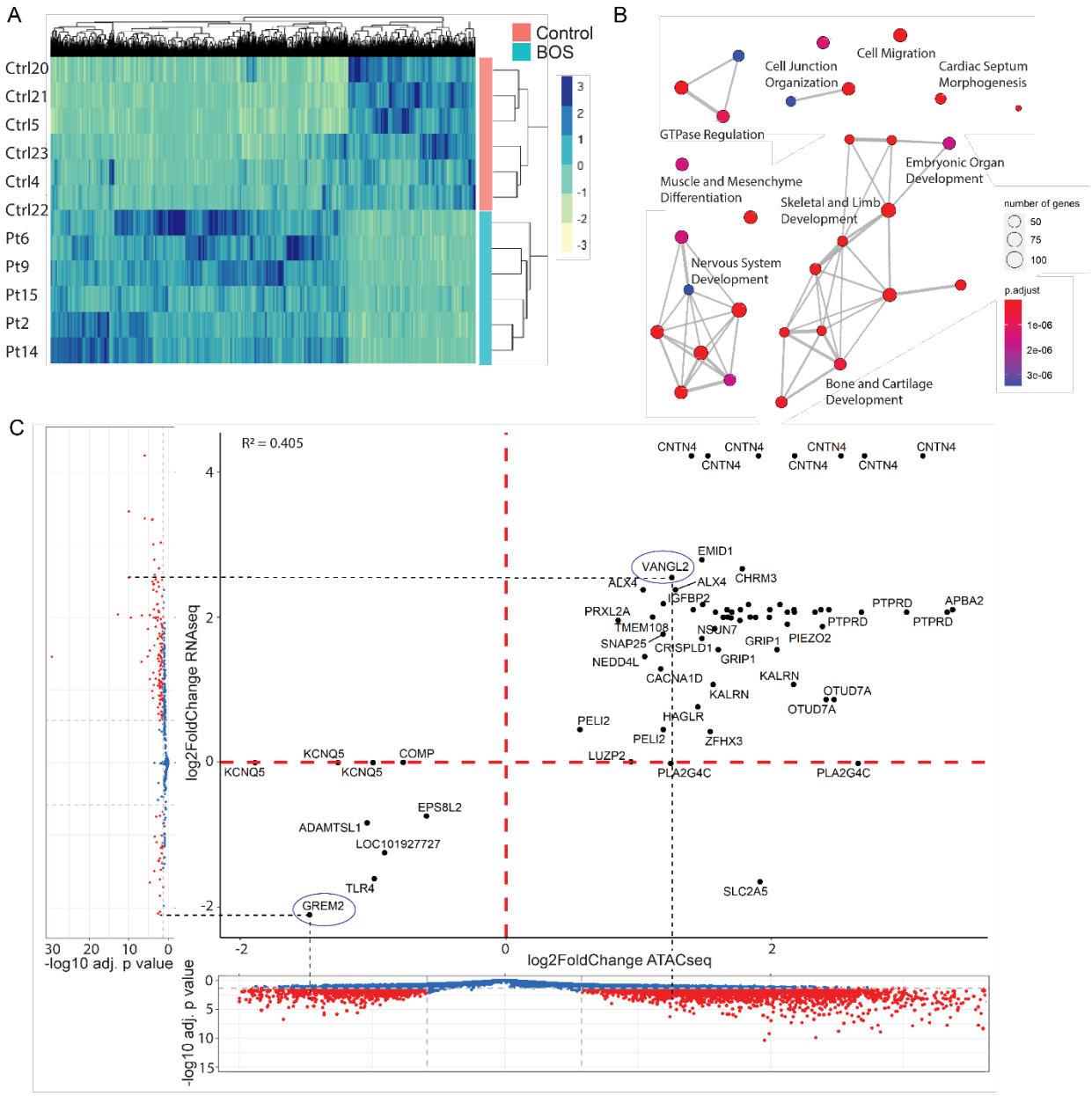

Figure 3: Epigenetic dysregulation in BOS patient-derived fibroblasts drive transcriptomic dysregulation. (A) ATACseq heatmap of all significant DEGs with adjusted p<0.05 and |log2FC|≥0.58 between BOS (blue, n=7) and control (pink, n=7) fibroblast found 4336 DEGs in fibroblast with 3036/4336 (70.0%) being more upregulated. **(B)** Gene set enrichment showed key dysregulated pathways, including nervous system development. **(C)** Integration of chromatin accessibility (ATACseq, x axis) and gene expression (RNA-seq, y-axis) in BOS patient (n=7) compared to control fibroblasts (n=7) identified a positive correlation (R^2=0.405) between chromatin accessibility and gene expression. We identified a set of 37 common dysregulated transcripts (right). DEGs were considered significant (red) for |log_2FC|>0.58 and adjusted p>0.05.

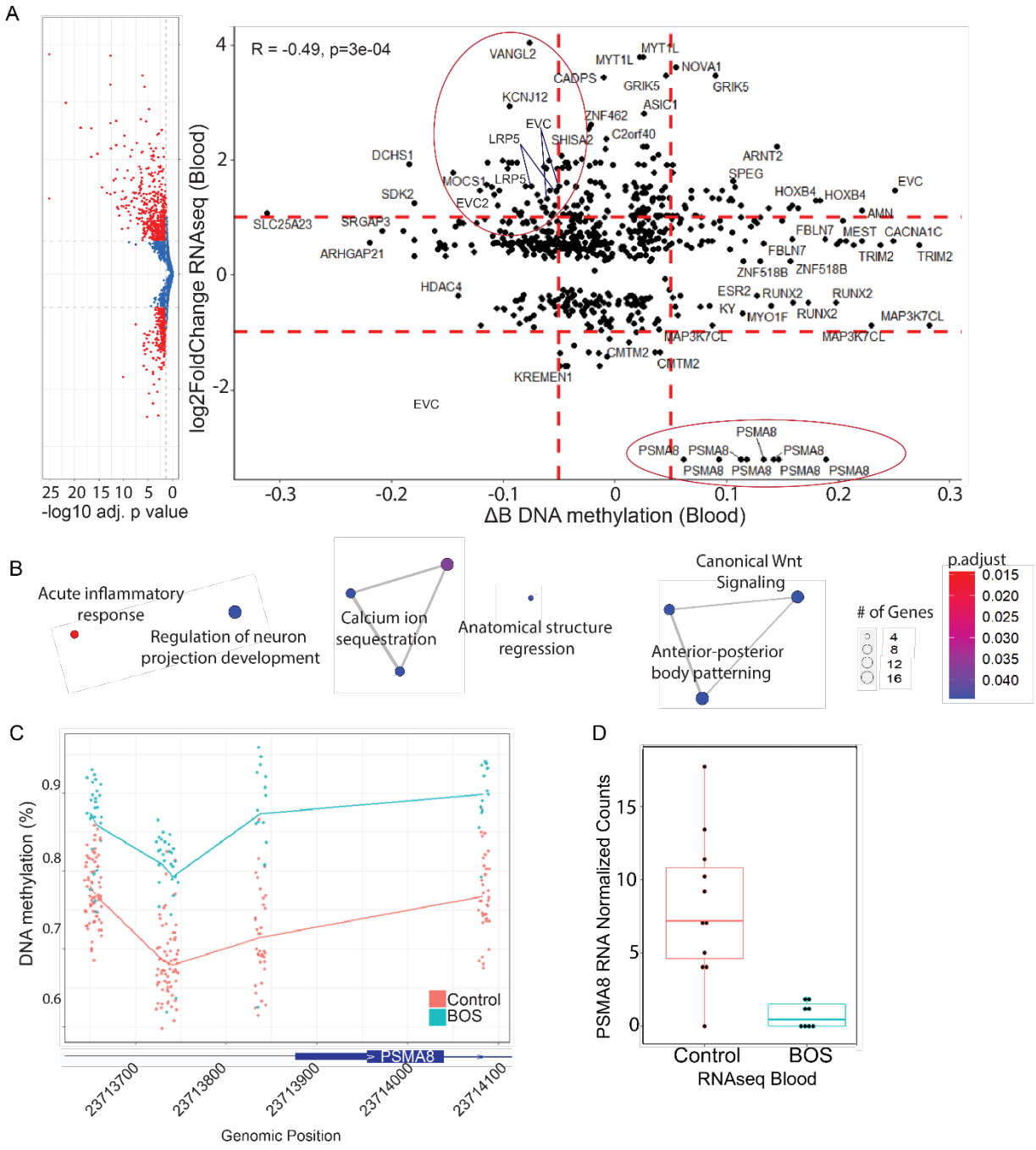

Figure 4: DNA methylation drives transcriptomic dysregulation in BOS samples and identifies common dysregulated transcripts enriched in Wnt signaling genes. (A) Integration of patient blood samples across DNAm (BOS n=13, control n=26) and RNA transcriptomic (BOS n=8, control n=11) dysregulation identifies 672 differentially methylated CpG sites (adjusted p<0.05) that correlated to 341 RNA-seq DEGs (adjusted p<0.05). These significant DEGs were further filtered for RNAseq $|\log_2 FC| \geq 0.58$, and DNAm $|\Delta\beta| \geq 0.05$, shown by the dotted red lines. After filtering, we retained 50/672 CpG sites (7.44%) and 24/341 unique genes (7.04%). **(B)** Analysis of enriched biological processes identified canonical Wnt signaling, anterior-posterior body patterning, regulation of neuron projection development and other biologically relevant pathways. **(C)** In BOS patients, *PSMA8*, a key component of the β-catenin destruction complex, is hypermethylated in blood DNAm across 8 CpG sites (Δβ 6.1% to 18.9%) and **(D)** shows strong

downregulation in blood RNA-seq (log_2FC=-2.92). Control sample normalized counts ranged from 0 to 17.7, with a mean of 8.1, and quartile bounds of 4.6 and 10.8. BOS normalized sample counts ranged from 0 to 2.1, with a mean of 0.8, and quartile bounds of 0 and 1.5.

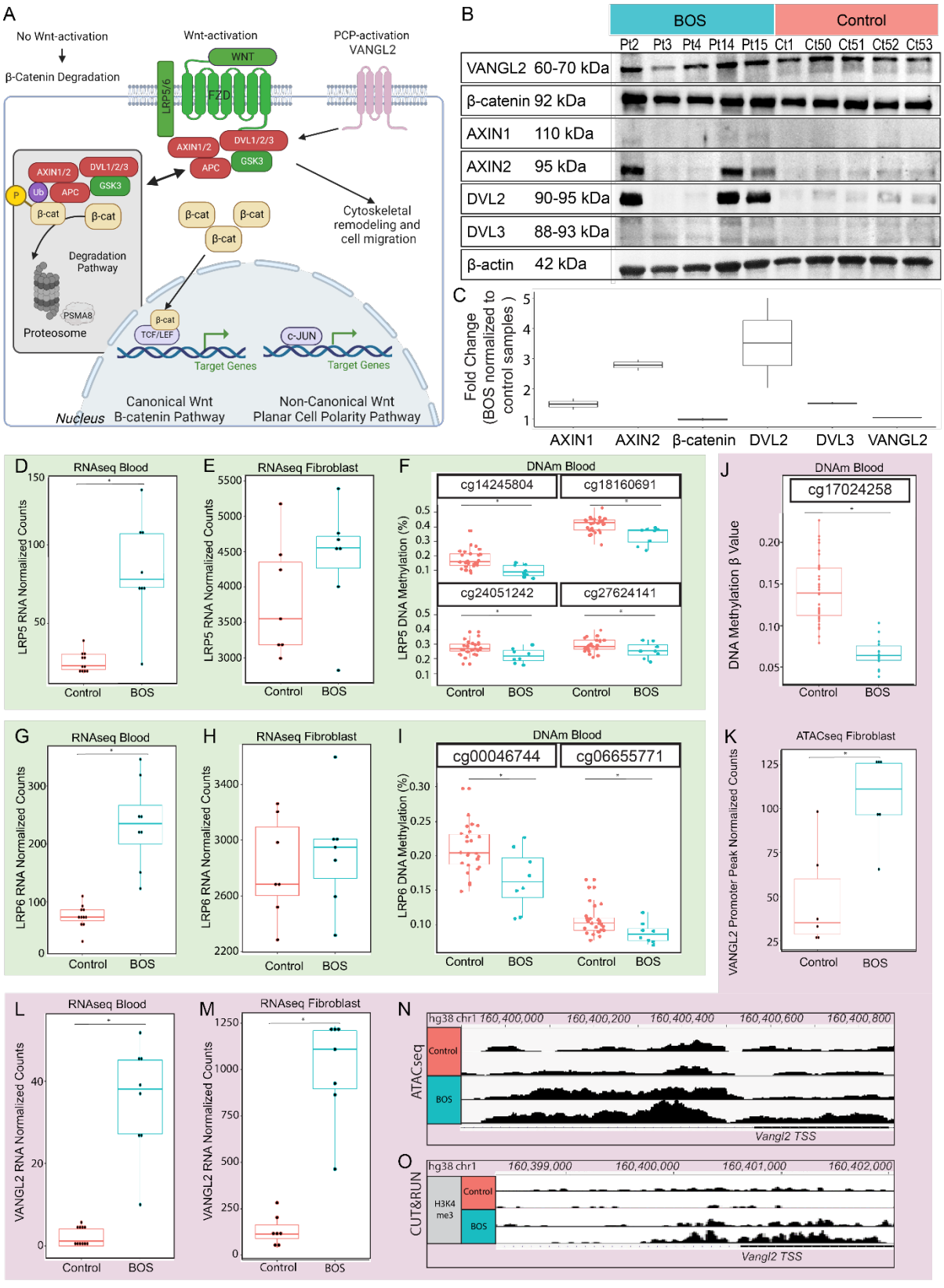

Figure 5: Truncated *ASXL1* dysregulates the canonical and non-canonical Wnt signaling pathways. (A) Canonical Wnt signaling pathway (left) is activated when Wnt ligand stimulates its receptors. This inactivates the "β-catenin destruction complex", allowing nuclear translocation of

β-catenin and activation of target genes. Van Gogh-like 2 (VANGL2) intersects with the canonical pathway through activation of Dishevelled (DVL) to activate non-canonical pathways (right) and cell migration. (B) Whole cell lysate (15ug) of representative BOS (n=5) and control-derived (n=5) fibroblasts show downstream Wnt pathway activation at the protein level through staining for VANGL2, β-catenin, axis-inhibition protein 1 (AXIN1), AXIN2, DVL2, and DVL3. (C) ImageJ quantification identified a fold increase of 1.5x for AXIN1, 2.8x for AXIN2, 3.5x for DVL2, and 1.5x for DVL3 averaged across BOS patient samples compared to controls. This was repeated 2 times.

In BOS patient samples, the Wnt pathway co-receptor *LRP5* (green) transcriptional upregulation in (D) blood (log2FC=1.64, p_{adj}=3.58x10-9) and (E) fibroblast RNA-seq and (F**)** DNA hypomethylation in blood (Δβ -3.5% to -8.0%, FDR<0.05) at multiple CpG sites. Similarly, *LRP6* (green) shows transcriptional upregulation in (G) blood RNA-seq (log2FC=1.63, p_{adj}=1.17x10-12) and (H) fibroblast RNA-seq and (I**)** DNA hypomethylation in blood (Δβ -2.7% to -4.0%, FDR<0.05)

BOS samples exhibit strong dysregulation of *VANGL2* across tissue and assay types (pink). For BOS samples, VANGL2 is (J) hypomethylated (Δβ -7.6%) at CpG site cg17024258, and shows (K) increased chromatin accessibility at the 5' UTR (log2FC=1.20). VANGL2 has significant transcriptional upregulation in (L) blood RNA-seq (log2FC=3.80) and (M) fibroblast RNA-seq (log2FC=2.55). In representative BOS patient samples, the *VANGL2* promoter shows **(N)** increased chromatin accessibility and **(O)** increased H3K4me3 marks compared to control.

Sample Group: Mean (Bounds) [Quartile]
LRP5 RNA-seq blood.
Control: 25.6 (18.3-39.1) [20.7-30.4]
BOS: 84.2 (24.1-134.6) [72.8-106.8]
LRP5 RNA-seq fibroblast.
Control: 3829 (2996-5177) [3187-4351]
BOS: 4392 (2824-5390) [4268-4719]
LRP6 RNA-seq blood.
Control: 75.0 (32.2-110.1) [67.8-86.6]
BOS: 234.5 (123.1-346.3) [199.9-266.9]
LRP6 RNA-seq fibroblast.
Control: 2804 (2286-3262) [2602-3094]
BOS: 2904 (2381-3596) [2725-3006]
VANGL2 RNA-seq blood.
Control: 2.3 (0-5.7) [0-4.1]
BOS: 35.3 (10.1-51.8) [27.2-45.2]
VANGL2 RNA-seq fibroblast.
134.8 (39.4-282.8) [90.8-163.4]
BOS: 1002.7 (464-1235.6) [894.7-1210.1]

Table 1: Integration of datasets across tissue types and across sample types identified a subset of overlapping genes that are significantly dysregulated in BOS.

These 7 genes were identified across blood and fibroblast RNA-seq as well as fibroblast ATACseq. Gene functions and their respective significant log2FC are shown.

Gene Name	Gene Function	log2 Fold Change		
		RNA-seq Blood	RNA-seq Fibro	ATACseq Fibro
VANGL2	Tissue polarity and patterning, and neural plate development	3.80	2.55	1.25
PRXL2A	Antioxidant activity and osteoclast differentiation	1.15	1.96	1.30
APBA2	Neuronal adapter protein	0.94	2.11	2.15
OTUD7A	Deubiquitinizing enzyme and potential tumour suppressor	0.90	0.86	2.44
KCNQ5	Potassium channel critical in neurons	0.65	-0.01	-1.39
PELI2	MAPK cascade, ubiquitin ligase activity	-0.37	0.45	0.87
GREM2	BMP antagonist, organogenesis and body patterning	-2.48	-2.11	-1.48